Variable Kinematics Layerwise Model for Analysis of Bonded Joints

Ugo Icardi and Federico Sola

***Abstract*— A displacement-based multi-layered zig-zag plate model with variable in-plane and through-the-thickness representation and fixed degrees of freedom is developed for analysis of bonded joints with laminated adherents. Characteristic feature, the in-plane representation can be varied across the adherents and the overlap to better simulate the variation of solutions and to satisfy the stress boundary conditions at the ends of the overlap. To this purpose, continuity functions are incorporated enabling the continuity of displacements and stresses where the representation is changed. Other continuity functions are included to allow an a priori fulfillment of the out-of-plane stress contact conditions at the interfaces of adjacent layers. High-order, through-the-thickness contributions are incorporated allowing the representation to be refined where step gradients rise. As the representation can vary from point to point, the present model permits an accurate analysis of laminates with general boundary conditions and of bonded joints under a unified approach. Applications are presented to sample cases of single- and double-lap joints taken from the literature. Specifically, three single-lap joints are considered, two of which with aluminum adherents and one with laminated composite adherents. Also a double-lap joint with aluminum adherents is analyzed. The numerical results show that accurate stress predictions are obtained with a low computational effort in all the cases considered using appropriate series expansions of displacements. The accuracy is good even using a single component in the expansion, which implies solving a 3x3 system.**

***Index Terms*— bonded joints; fixed d.o.f.; high-order hierarchic representation; zig-zag model**

I. Introduction

BONDED joints are characterized by improved accommodation of thermal expansion mismatch and hygrothermal swelling, improved vibration isolation and sealing with respect to traditional mechanical fastening. In addition, adhesive bonding gives a gradual transfer of load between the structural elements and, therefore, a more uniform stress distribution within the joint, which can thus have better strength and an improved fatigue life. On the contrary, bolted/riveted joints can determine the growth of strong stress concentrations, as a consequence of the material discontinuities that characterize the construction. Bonding also offers better aerodynamic capabilities and better aesthetic appearance, along with reduced tooling and machinery costs and improved manufacturability.

All these aspects have contributed to the spread of bonded joints in many engineering fields. In addition, as claimed by Her [1], adhesive bonding is the best technology for joining composites, since these materials can suffer from catastrophic microstructural failures in service, which can be triggered off by the stress concentrations due to mechanical fastening.

The behavior of bonded joints requires in many cases to be simulated taking into consideration stress boundary conditions in a point form, material and geometric nonlinearity and finally to accurately model the out-of-plane stress and strain fields. Without paying attention to these aspects, the joint strength could not be accurately predicted, thus preventing from the design of safe bonded structures. The comprehensive literature reviews by Vinson [2], He [3] and da Silva et al. [4] bears witness to the interest that the fully understanding of the behavior of bonded joints has aroused within the researchers. In details, the evaluation of the stress and strain fields across the joint and how they are influenced by geometry, materials, loading conditions, temperature and moisture effects represent the main topics addressed.

As a corroboration of the complexity to simulate the behavior of bonded joints, it is underlined that, even when the adherents and the adhesive materials are considered as isotropic and homogeneous, analytical [5]-[7], finite element [8]-[10] and finite difference [11] solutions predict intricate stress and deformation fields. This is a consequence of the differences between the elastic moduli of adhesive and adherents and of the enforcement of stress boundary and loading conditions. In fact, the progressive reduction of the strain in the adherents along the overlap and the continuity of the adhesive/adherents interface determine non-uniform shear strain and stress distributions in the adhesive layer. In addition, the out-of plane transverse shear and normal stresses in single- (SLJ) and double-lap (DLJ) bonded joints reach a peak close to the edges of the bonding layer, which can determine a premature failure of the joint during the service life. As shown, e.g., by Nemes and Lachaud [12], the peeling stress can become the dominant effects at the edges, since it can be larger

Manuscript received October 10, 2013.

Ugo Icardi is Associate Professor at Politecnico di Torino - Dipartimento di Ingegneria Meccanica e Aerospaziale - Corso Duca degli Abruzzi 24, 10129 Torino, Italy (corresponding author to provide phone: +39 (0)110906872; fax: +39 (0)110906899; e-mail: ugo.icardi@polito.it).

Federico Sola is PhD student at Politecnico di Torino - Dipartimento di Ingegneria Meccanica e Aerospaziale - Corso Duca degli Abruzzi 24, 10129 Torino, Italy (e-mail: federico.sola@polito.it).

DOI: 10.5176/0000-0004_1.1.2

than the shear stress. Non classical problems, such as complex loading schemes and the damage formation have been also treated during years. As examples, the paper by Sayman et al. [13] dealing with joint undergoing impact loading and that by Kim [14] dealing with interface crack in a single lap joint are cited. A number of approaches aimed at improving the performances of bonded joints have been suggested. For instance, da Silva and Adams [15] proposed a technique based on internal taper and adhesive fillet arrangement to reduce the peel stress, while Quaresimin and Ricotta [16] proved that that the fatigue strength can be improved adopting long overlap length and spew fillet corner geometry.

Finite element methods are extensively employed for simulating the behavior of joints since they can carry out analysis of complex joint geometries and complex material models including nonlinear effects, without setting any simplifying assumption, which could affect accuracy. As finite element analyses (FEA) require large computing time and quite long preparation, analytical models (AM) based on simplifying assumptions are often used as alternatives. He [3] and da Silva et al. [4] provide a thorough discussion of AM, and an assessment of their characteristics when studying joints. In order to obtain a fast, low cost solution in closed form, many AM are stress-based models, which still include some of the simplifying hypotheses of the pioneering models by Volkersen [17], Goland and Reissner [18] and Hart-Smith [19]. Therefore, many times, they assume a shear stress that is constant across the thickness of the adhesive, or they suppose that the adhesive can deform only in shear and the adherents are rigid, thus obtaining shear and peel stresses in the adhesive layer through the solution of a plane strain problem.

As all these simplifying hypotheses can be far from reality, more detailed models have been proposed over the years trying to consider the effects due to the deformation of the adherents and of the adhesive. However some effects such as the stress-free boundary conditions at the ends of the overlap, or the bending effect due to the eccentric load path of SLJ and the deformability of adherents are still disregarded or accounted for with simplified techniques (see, e.g. [18] and [19]) in order to limit the computational effort. For instance, a transverse load factor and a bending load factor are calculated in order to relate the applied tensile load to the bending moment and to the transverse force at the ends of the overlap. In this way, it is possible to solve the nonlinear geometric problem as a linear problem applying bending and transverse loads in addition to the tensile load.

It was only the advent of bonded laminated composites as primary structures in the 80's that boosted the development of more complex AM together with an increasing number of three-dimensional (3-D) FEA. In fact, as outlined in Ref. [20], these kind of materials calls for an accurate simulation of the warping, shearing and straining deformations of the normal and out-of-plane stresses that rise as a consequence of the different mechanical properties of constituent layers and of the relatively poor out-of-plane moduli and strengths of the laminate construction. Diaz et al. [10] provides the full list of the most diffused finite element models and presents 3-D FEA of SLJ with CFRP adherents and epoxy adhesive. Pearson and Mottram [9] deals with 3-D FEA of the non-linear stiffness characteristics of adhesively bonded SLJ, while Andruet et al. [8] is cited as example of paper treating geometric nonlinearity.

A first alternative to this approach is that of Xu and Li [10], which solved the 3-D differential governing equations of a tubular bonded joint through a finite- difference scheme. Another alternative is to employ refined analytical bonded joint models, whose complexity determines whether it is possible to obtain solutions in closed or numerical form. Gustafson et al. [5] and Radice and Vinson [7] exhaustively review these models. The approaches by Renton and Vinson [21] and Srinivas [22] are cited as examples accounting for the transverse shear and normal deformations of adhesive and adherents and satisfying the stress-free boundary conditions. Instead, the model by Allman [23] is an example, which considers the effects of bending, stretching and shearing in the adherents and the tearing actions in the adhesive. Even if refined AM with a complex representation cannot always obtain a closed form solution, as discussed by Adams and Mallick [24], they are not disadvantageous and unpractical compared to simpler models, since they reduce costs with respect to 3-D FEA without any accuracy loss. In addition, refined AM are not affected from the stress singularities at the edge interfaces like 3-D FEA. The paper by Yousefsani and Tahani [6] is mentioned as example of application of a modern, efficient and accurate stress-based layerwise plate theory to the analysis of DLJ.

Within the framework of AM, the application of displacement-based models such as those by Mortensen and Thomsen [25], Zou et al. [26] and Yang and Pang [27] opens the possibility for the development of models that enable to carry out analyses of bonded joints and laminates under a unified approach. The advantages of this achievement are plain; in fact, it would enable the designers to perform realistic analysis of the structures in the bonded region and outside it contemporaneously and with the same tool. In addition, it is worthwhile to mention that the most widespread shell finite elements and analytical tools currently employed by the industries derive from displacement-based models. The above mentioned applications of Refs. [25], [26] and [27] employ the Classical Laminated Plate Theory (CLPT), or the First-Order Shear Deformation Plate Theory (FSDPT) to perform the analysis, even if the kinematics of these models cannot accurately describe the stress fields across the thickness of bonded materials with distinctly different mechanical properties. In fact, the adhesive peel stress is neglected in the constitutive equations and the transverse shear stress is disregarded or assumed constant across the thickness. Therefore, equilibrium is not satisfied at the interfaces and the stress free conditions at the end of the overlap are not met. However, despite these violations, the results can be in a good

agreement with those of finite element models, as shown e.g. in [27].

From this brief discussion it seems evident the lack of refined displacement-based models that can be conveniently applied to the analysis of bonded joints as they can treat local and global scale problems with the same tool. Namely, bonded joints with laminated adherents can be analyzed with the same model used elsewhere. With the aim to contribute to fill this gap, the zig-zag plate model with variable kinematics and fixed number of functional degrees of freedom (d.o.f.) recently developed in Ref. [28], is here particularized to the analysis of bonded joints. As shown by the successful applications presented in Refs. [28] and [29], the model can easily satisfy any kind of boundary conditions thanks to a variable kinematics, however in order to fulfill the continuity conditions where the in-plane representation step-varies (e.g. between the adherent and the overlap) new contributions have to be added. Aiming at keeping as lower as possible the computational burden, the model has just five primary generalized displacement variables, the same as FSDPT, while all the expressions of high-order contributions and continuity functions are calculated apart in closed form as functions of the d.o.f. using a symbolic calculus tool. This ploy enables to overcome the intricacies of manipulating a rather complex and cumbersome algebra and to consistently speed-up computations, as a refinement of the model does not determine an increase of the memory storage dimension and of the processing time.

The paper is structured as follows. First, the loading and boundary conditions requirements are discussed in order to explain the assumptions of the model. Then, numerical results aimed at showing the capabilities of the present model are shown. Applications are presented to sample cases for which the results by finite element analyses or by analytical models are available for comparisons. Finally, the performances of the present model are discussed and the pertinent conclusions are outlined.

II. Structural model

In order to put the article in the right perspective, a brief review about the model used for the analysis of joints and the requirements needed to accurately simulate their response is premised along with a discussion of the most widespread approach adopted to account for the layerwise effects that rise in multilayered structures. The readers can find more exhaustive discussions about these topics in the papers by da Silva et al. [4] and by Kapuria and Nath **Error! Reference source not found.**.

The most widespread approach is that of stress based and mixed models, which assume the displacements separately from the stresses, adopting appropriate self-equilibrating representations which usually have a number of unknowns that increases with the number of physical or computational layers. This representation is extensively adopted, since it does not require complex algebraic manipulations to obtain stresses from strains, thus it is easy to develop. However this choice implies a high computational burden, because usually the unknowns depend on the number of layers. On the contrary, displacement-based models assume a representations that *a priori* fulfils the conditions on stresses, and thus it involve a fixed number of unknowns even though quite intricate algebraic operations are required to obtain closed form expressions of the high-order terms. Displacement-based models find many applications for the development of finite elements used in the analysis of composites, but they are infrequently adopted for studying joints, since the stress boundary conditions cannot be easily enforced.

However, whatever the modelling approach chosen is, the analysis of joints requires to correctly describe out-of-plane stresses and to have the displacements continuous at the interfaces of the layers constituting the adherents and at the interfaces between adherents and bonding film. Accordingly, piecewise continuous functions with appropriate discontinuous derivatives at the layer interfaces should be employed to represent the displacements, in order to respect the equilibrium condition, which implies the fulfilment of the continuity requirements for out-of-plane stresses. As far as AM are concerned, it is mandatory to evaluate their performances at the light of accuracy and costs. Models with a variable number of d.o.f. generally provide better accuracy, as they can refine their representation in regions with step gradients. However, such models could have processing time and memory storage dimension too large for an extensive application in the industrial environment. On the other hand, the models with fixed d.o.f. are efficient but not always their accuracy is satisfactory as they adopt a too simplified modelling approach.

In order to overcome this drawback, the model of Ref. [28], which is here particularized to the analysis of joints, adopts a variable kinematics whose terms are calculated apart once at a time as function of the d.o.f. that are the three displacements and the two rotations of the normal of the reference plane. Previous applications in Refs. **Error! Reference source not found.** and [29] showed that this model can accurately describe directly from constitutive equations the stress fields of laminates and sandwiches even when the variation of their mechanical properties is intricate. In the refined version for the analysis of joints here presented, a new set of continuity functions is added aiming at fulfilling the displacement and stress continuity conditions at the interfaces of the adjacent regions where the in-plane representation is varied moving over the plane of the joint.

Like its previous version [28], the model is still based on a piecewise representation of displacements that includes a contribution with fixed expansion order across the thickness, contributions with a variable order of representation and finally contributions with piecewise variation across the thickness. It is reminded that the terms with variable order of representation are incorporated to enable the fulfilment of the equilibrium conditions and the boundary conditions prescribed

by the elasticity theory, while the contributions with piecewise variation across the thickness are aimed at *a priori* fulfilling the stress and displacement continuity conditions at the layer interfaces.

As for the previous version [28], all the higher-order contributions and the continuity functions are calculated apart once at a time obtaining their expressions in terms of the functional d.o.f. with a symbolic calculus tool. In this way, the present model can refine the representation across the thickness just imposing the equilibrium conditions in more points, but keeping fixed the number of d.o.f. As a consequence, refinement can be obtained without increasing the memory storage dimension or the processing time, differently from finite element models and analytical models with a variable number of d.o.f. In fact, for instance, 3D FEA requires a very fine meshing for keeping a reasonable aspect ratio of solid elements across the thickness of the adhesive film, resulting into a large computational effort.

It is also remarked that the present version of the model offers the possibility to perform analysis of laminates and of multi-layered bonded structures under a unified approach in which the in-plane representation can vary in a step way moving in the in-plane direction across the joint.

For what concerns the analysis of bonded joints with laminated adherents, many times the solution of a multiple-point boundary value problem is required. In this section, the imposed boundary conditions for studying joints are briefly summarized, while in Section 2.3.2, more specific details about the procedure adopted to obtain closed form relations through symbolic calculus are provided. Here, it is just reminded that by the viewpoint of the computation of the unknowns coefficients, imposing Eqs. (1) – (3) is equivalent to impose Eqs. (36) – (39).

As far as the boundary conditions at the edges of the adherents and of the overlap regions are concerned, they are satisfied calculating appropriate expressions of the coefficients of higher-order contributions to displacements of Eqs. (10) – (12), as follows. Specifically, if one assumes that no variation occurs in the transverse direction *y* as customarily, the boundary conditions require that the transverse shear and the normal stresses should identically vanish over the free surface Ω_1 and Ω_2 of the overlap (see Figure 1). Thus it is possible to enforce the following relations to hold:

$$\sigma_{xz} = 0; \quad \int_{\Omega_i} \sigma_{xz} dz = 0; \quad \sum_k \int_{\Omega_k} \sigma_{xz} dz = 0; \tag{1}$$

$$\sigma_{xx} = 0; \quad \int_{\Omega_i} \sigma_{xx} dz = 0; \quad \sum_k \int_{\Omega_k} \sigma_{xx} dz = 0; \tag{2}$$

if we want the satisfaction at a specific point across the thickness, in integral form over the surface Ω_i or over all the sub-regions of Ω_k and Ω_i, respectively.

In a similar way, the stresses can be imposed to be consistent with the applied loads

$$N = \int_{\Omega_i} \sigma_{xx} dz = -\int_{\Omega_i} \sigma_{xz} dx; \tag{3}$$

$$M = \int_{\Omega_i} z\, \sigma_{xx} dz;$$

$$Q = \int_{\Omega_i} \sigma_{xz} dz;$$

Where *N*, *M*, *Q* are the in-plane, bending and shear resultants.

As mentioned above, the in-plane representation of displacements is allowed to step-vary in the in-plane direction of the joint since different constraints should be satisfied in different regions, due to the change of geometry and material properties across the joint. In order to fulfil the appropriate continuity requirements at the in-plane interfaces, the continuity functions of Eqs. (20) – (22) are incorporated in the displacement field. In this way, the model can easily treat joints, which have a step-way variation of the trial functions (43) – (47) moving in the in-plane direction. The new set of continuity functions also enables to refine the representation of the model in the in-plane direction.

A distinctive feature of the model [28] is represented by the possibility of enforcing a non-vanishing transverse shear at clamped edges even when the mid-plane displacements and shear rotations are forced to vanish. In this way, one of the drawback of the models with mid-plane displacements and shear rotations as functional d.o.f is overcome. Similarly, non-vanishing stresses can be enforced, even when the trial functions for the displacements *a priori* fulfil the previous conditions of Eqs. (1) and (2), since in real adhesive joints a fillet of surplus adhesive, the so-called spew-fillet can be formed at the end of overlap zone allowing to transfer the shear stress.

In addition, the model can be made consistent with a state of nonzero transverse normal stress with a nonzero bending strain in the thick regime and with a state of zero transverse shear stress in presence of nonzero bending strain in the thin regime.

Finally it could be noticed that, any other condition enforced in the reference papers considered for comparisons can be easily fulfilled, as this only means a variation in the conditions employed to get appropriate closed form expressions of higher-order coefficients of displacements through symbolic calculus.

A. Notations

It is postulated the hypothesis that the overlap and the adherents can be treated as laminates. In order to take into consideration that the adherents may have a different number of layers, the structural model simulates the joint as a laminate whose number of layers is that of the overlap, as shown in Figure 1. As a consequence, bonded joints with laminated adherents are treated as plates with a different number of layers that has different material properties. Obviously, the properties of some layers of the adherents are assumed to vanish, because just the overlap has the whole set of layers.

The plate reference surface is the middle surface Ω of the

overlap. The plate is considered to be made of *N* orthotropic layers, perfectly bonded together, with their principal material directions arbitrarily oriented and with material properties entirely different each other. The reference system adopted is a rectangular Cartesian reference frame (*x, y, z*) with (*x, y*) in Ω and *z* normal to it. The symbols $^{(k)}z^{+}$ and $^{(k)}z^{-}$ indicates the position of the upper^{+} and lower $^{-}$ surfaces of the generic k^{th} layer, while the superscript $^{(k)}$ is applied to all the quantities that belong to a generic layer *k*. The displacements in the *x, y* and *z* directions are indicated respectively as *u*, *v* and *w*. They are described as the sum of fixed contributions $\hat{U}^0$, $\hat{V}^0$, $\hat{W}^0$, high-order contributions $\hat{U}^{ho}$, $\hat{V}^{ho}$, $\hat{W}^{ho}$ and piecewise contributions $\hat{U}^c$, $\hat{V}^c$, $\hat{W}^c$, $\hat{U}^{ic}$, $\hat{V}^{ic}$, $\hat{W}^{ic}$ as discussed forward. The functional d.o.f. are the in-plane displacements of the points over the middle plane Ω u^0 *(x, y)* and v^0 *(x, y)*, the transverse displacement w^0 *(x, y)* and the shear rotations of the normal γ_x^0 *(x, y)*, γ_y^0 *(x, y)* to these points. The strains are indicated as ε_{ij} and the stresses as σ_{ij} *(i, j≡ x, y, z)*.

Linear strains ε_{ij} are assumed within the paper, but the effects of geometric nonlinearity are taken into consideration adopting the updated Lagrangian methodology, which computes the strains at each new loading step from the configuration at the previous step, instead of calculating them from the initial unloaded configuration. This approach is more numerically efficient than the standard Lagrangian approach, which calls for the application of nonlinear stress-strain relations and the solution of non-linear equations.

B. Kinematics

Four separated contributions are included in the through-the-thickness variation of displacements across the thickness, which is postulated in the following general, piecewise form:

$$u(x,y,z) = \hat{U}^0(x,y,z) + \hat{U}^{ho}(x,y,z) + \\ + \hat{U}^c(x,y,z) + \hat{U}^{ic}(x,y,z) \tag{4}$$

$$v(x,y,z) = \hat{V}^0(x,y,z) + \hat{V}^{ho}(x,y,z) + \\ + \hat{V}^c(x,y,z) + \hat{V}^{ic}(x,y,z) \tag{5}$$

$$w(x,y,z) = \hat{W}^0(x,y,z) + \hat{W}^{ho}(x,y,z) + \\ + \hat{W}^c(x,y,z) + \hat{W}^{ic}(x,y,z) \tag{6}$$

The previous version [28] of the model already includes the first three contributions, which are $(\,)^0$, $(\,)^{ho}$ and $(\,)^c$, while here in order to enable the analysis of adhesively bonded joints the new contributions $(\,)^{ic}$ are added. The terms with superscript 0, which are here indicated as $\wp^0$, have a polynomial representation with a fixed expansion order across the thickness. In details, they are:

$$\hat{U}^0(x,y,z) = u^0(x,y) + z(\gamma_x^0(x,y) - w^0{}_{,x}) \tag{7}$$

$$\hat{V}^0(x,y,z) = v^0(x,y) + z(\gamma_y^0(x,y) - w^0{}_{,y}) \tag{8}$$

$$\hat{W}^0(x,y,z) = w^0(x,y) \tag{9}$$

These terms contain just the primary, starting contributions expressed in terms of the functional d.o.f., which are the same of FSDPT model.

The terms $\wp^{ho}$ with the superscript *ho* can vary from point to point across the thickness, therefore they allow obtaining a variable kinematics across the thickness. These terms are aimed at fulfilling any possible set of boundary conditions, since they provide a variable order of representation across the thickness. Specifically, the right expansion order can be set in any region, in order to have enough unknown coefficients to be determined enforcing the fulfilment of the prescribed boundary conditions at any point in the plane and across the thickness. Their expressions are postulated as follows:

$$\hat{U}^{ho}(x,y,z) = A_{u2}(x,y)z^2 + ... + A_{un}(x,y)z^o \tag{10}$$

$$\hat{V}^{ho}(x,y,z) = A_{v2}(x,y)z^2 + ... + A_{vn}(x,y)z^o \tag{11}$$

$$\hat{W}^{ho}(x,y,z) = A_w(x,y)z + ... + A_{wn}(x,y)z^o \tag{12}$$

It is underlined that Eqs. (10) – (12) are valid only within a single physical or computational layer. Despite this, the functional d.o.f. of the present model are fixed, since the expressions of the terms $\wp^{ho}$ are calculated apart once at a time as functions of the d.o.f. The aim of these terms is to obtain a variable representation from point to point across the thickness, so they are "*adaptive*" contributions that enable the model to be refined in the regions with step gradients and allow it to account for the variation of the material properties. As a consequence of their presence, the representation can adapt to the variation of solutions, thus getting accurate stress predictions directly from constitutive equations, even for thick structures with abruptly changing material properties.

As mentioned above, the expressions of the terms in Eqs. (10) – (12) are computed enforcing the boundary conditions of the joint (Eqs. (1) – (3)), the stress-free boundary condition at the upper and lower bounding faces (Eqs. (36) – (39)) and, finally, the equilibrium conditions (Eqs. (40)) at specific points across the thickness. The enforcement of all these constraints determines cumbersome algebraic manipulations, which are here avoided carrying out these computations with a symbolic calculus tool, thus overcoming the main drawback of this kind of models.

The function of the terms $\wp^c$ with the superscript *c* is to *a priori* satisfy the continuity conditions as prescribed by the elasticity theory for keeping equilibrium at the interfaces between different layers. Their expressions are the following:

$$\hat{U}^c(x,y) = \sum_{k=1}^{n_i} \Phi_x^k(x,y)(z - z_k)H_k + \sum_{k=1}^{n_i} C_u^k(x,y)H_k \tag{13}$$

$$\hat{V}^c(x,y) = \sum_{k=1}^{n_i} \Phi_y^k(x,y)(z - z_k)H_k + \sum_{k=1}^{n_i} C_v^k(x,y)H_k \tag{14}$$

$$\hat{W}^c(x,y)=\sum_{k=1}^{n_i}\Psi^k(x,y)(z-z_k)H_k \\ +\sum_{k=1}^{n_i}\Omega^k(x,y)(z-z_k)^2H_k+\sum_{k=1}^{n_i}C_w^k(x,y)H_k \quad (15)$$

Where H_k is the Heaviside unit step function that triggers the contribution of the continuity functions from the pertinent interface.

The functions Φ_x^k, Φ_y^k are aimed at satisfying the continuity of the out-of-plane shear stresses

$$\sigma_{xz}\big|_{(k)_{z^+}}=\sigma_{xz}\big|_{(k)_{z^-}} \quad (16)$$

$$\sigma_{yz}\big|_{(k)_{z^+}}=\sigma_{yz}\big|_{(k)_{z^-}} \quad (17)$$

Their presence is a common feature of all the zig-zag models and it makes the in-plane displacements continuous. As they produce appropriate discontinuous derivatives across the thickness, they determine an *a priori* fulfilment of the stress continuity conditions.

Non classical feature, the transverse displacement embodies two zig-zag contributions Ψ^k, Ω^k whose goal is to meet the stress contact conditions on the transverse normal stress and its gradient:

$$\sigma_z\big|_{(k)_{z^+}}=\sigma_z\big|_{(k)_{z^-}} \quad (18)$$

$$\sigma_{z,z}\big|_{(k)_{z^+}}=\sigma_{z,z}\big|_{(k)_{z^-}} \quad (19)$$

Eqs. (18) - (19), which are directly obtained from the local equilibrium equations, should be fulfilled since the transverse normal stress σ_z and the related strain ε_z have a central role for keeping equilibrium of bonded joints with laminated adherents. Finally, C_u^k, C_v^k and C_w^k make continuous the displacements at the points across the thickness where the representation is varied.

The aim of last contributions $\wp^{ic}$ is to enable the representation of the d.o.f. to be freely changed over the plane *(x, y)*. In fact, these terms satisfy the displacement and stresses continuity conditions at the interfaces of adjacent regions across which the in-plane representation is varied in a step-way moving across the joint. This aspect is of primary importance, since the contributions $\wp^0$ defined above can have an in-plane representation that changes moving along the in-plane coordinate of the joint. In fact, their trial functions can be different in order to fulfil specific boundary conditions in different regions. The terms $\wp^{ic}$ are:

$$\hat{U}^{ci}(x,y)=\Theta_x^k(x,y)(x-x_k)H_k+ \\ +\Gamma_x^k(x,y)(x-x_k)^2H_k \quad (20)$$

$$\hat{V}^{ci}(x,y)=\Theta_y^k(x,y)(x-x_k)H_k+\Gamma_y^k(x,y)(x-x_k)^2H_k \quad (21)$$

$$\hat{W}^{ci}(x,y)=\left(\Theta_w^k+\Theta_{w*}^k+\chi_w^k+\chi_{w*}^k\right)(x,y)(x-x_k)H_k+ \\ +\left(\Gamma_w^k+\Gamma_{w*}^k+\Lambda_w^k+\Lambda_{w*}^k\right)(x,y)(x-x_k)H_k \quad (22)$$

Once again, H_k activates the contribution of the continuity functions starting from the point where the in-plane representation varies. It could be underlined that this variation is not possible in both directions, but it can happen only in one (x or y). The goal of the terms of first order in the in-plane coordinate is to satisfy the continuity of the stresses, while the continuity of their gradient is fulfilled with the terms of second order in *x*.

Similarly to the high order terms, the explicit expressions of the continuity functions are evaluated in closed form using a symbolic calculus tool, following the procedure outlined hereafter.

C. Continuity functions and hierarchic terms

The closed form expressions of the continuity functions and of the hierarchic contributions are obtained as follows.

1) Continuity functions

The displacement continuity functions C_u^k, C_v^k and C_w^k, which make continuous the displacements at the points across the thickness where the representation is varied, do not involve derivatives of the functional d.o.f. of any order, as it can be seen in a straightforward way enforcing the continuity of displacements at the interfaces of the regions where the representation is varied. Their expressions at a generic interface $\Im$ are obtained directly as:

$$C_u^k(x,y)=\hat{U}_k^{ho}(x,y,z_\Im)-\hat{U}_{k+1}^{ho}(x,y,z_\Im) \quad (23)$$

$$C_v^k(x,y)=\hat{V}_k^{ho}(x,y,z_\Im)-\hat{V}_{k+1}^{ho}(x,y,z_\Im) \quad (24)$$

$$C_w^k(x,y)=\hat{W}_k^{ho}(x,y,z_\Im)-\hat{W}_{k+1}^{ho}(x,y,z_\Im) \quad (25)$$

The other continuity functions have more intricate expressions, however it is possible to notice that Φ_x^k, Φ_y^k and Ψ^k contain first order derivatives of the functional d.o.f., whereas Ω^k involves also second order derivatives of the functional d.o.f. In order to take into consideration these aspects, their expressions are assumed in the following form:

$$\Phi_x^k=\mathbf{\Phi}_{u1}^{(k)}\left(\hat{U}^0+\hat{U}^{ho}\right)_{,x}+\ldots+\mathbf{\Phi}_{u9}^{(k)}\left(\hat{W}^0+\hat{W}^{ho}\right)_{,z} \quad (26)$$

$$\Phi_y^k=\mathbf{\Phi}_{v1}^{(k)}\left(\hat{U}^0+\hat{U}^{ho}\right)_{,x}+\ldots.+\mathbf{\Phi}_{v9}^{(k)}\left(\hat{W}^0+\hat{W}^{ho}\right)_{,z} \quad (27)$$

$$\Psi^k=\mathbf{\Psi}_1^{(k)}\left(\hat{U}^0+\hat{U}^{ho}\right)_{,x}+\ldots+\mathbf{\Psi}_9^{(k)}\left(\hat{W}^0+\hat{W}^{ho}\right)_{,z} \quad (28)$$

$$\Omega^k=\mathbf{\Omega}_1^{(k)}\left(\hat{U}^0+\hat{U}^{ho}\right)_{,xx}+\ldots+\mathbf{\Omega}_{18}^{(k)}\left(\hat{W}^0+\hat{W}^{ho}\right)_{,zz} \quad (29)$$

$\Phi_{u1}^{(k)}$, ..., $\Omega_{18}^{(k)}$ are the so-called continuity coefficients, which depend only on the elastic properties of the constituent layers. They multiply derivatives of the displacements according to the following scheme:

$$\begin{aligned}
&\Phi_{u1}^{(k)} \to \left(\hat{U}^0 + \hat{U}^{ho}\right)_{,x} \quad \Phi_{u2}^{(k)} \to \left(\hat{U}^0 + \hat{U}^{ho}\right)_{,y} \\
&\Phi_{u3}^{(k)} \to \left(\hat{U}^0 + \hat{U}^{ho}\right)_{,z} \quad \Phi_{u4}^{(k)} \to \left(\hat{V}^0 + \hat{V}^{ho}\right)_{,x} \\
&\Phi_{u5}^{(k)} \to \left(\hat{V}^0 + \hat{V}^{ho}\right)_{,y} \quad \Phi_{u6}^{(k)} \to \left(\hat{V}^0 + \hat{V}^{ho}\right)_{,z} \\
&\Phi_{u7}^{(k)} \to \left(\hat{W}^0 + \hat{W}^{ho}\right)_{,x} \quad \Phi_{u8}^{(k)} \to \left(\hat{W}^0 + \hat{W}^{ho}\right)_{,y} \\
&\Phi_{u9}^{(k)} \to \left(\hat{W}^0 + \hat{W}^{ho}\right)_{,z}
\end{aligned} \tag{30}$$

$$\begin{aligned}
&\Psi_{1}^{(k)} \to \left(\hat{U}^0 + \hat{U}^{ho}\right)_{,x} \quad \Psi_{2}^{(k)} \to \left(\hat{U}^0 + \hat{U}^{ho}\right)_{,y} \\
&\Psi_{3}^{(k)} \to \left(\hat{U}^0 + \hat{U}^{i}\right)_{,z} \quad \Psi_{4}^{(k)} \to \left(\hat{V}^0 + \hat{V}^{ho}\right)_{,x} \\
&\Psi_{5}^{(k)} \to \left(\hat{V}^0 + \hat{V}^{ho}\right)_{,y} \quad \Psi_{6}^{(k)} \to \left(\hat{V}^0 + \hat{V}^{ho}\right)_{,z} \\
&\Psi_{7}^{(k)} \to \left(\hat{W}^0 + \hat{W}^{ho}\right)_{,x} \quad \Psi_{8}^{(k)} \to \left(\hat{W}^0 + \hat{W}^{ho}\right)_{,y} \\
&\Psi_{9}^{(k)} \to \left(\hat{W}^0 + \hat{W}^{ho}\right)_{,z}
\end{aligned} \tag{31}$$

$$\begin{aligned}
&\Omega_{1}^{(k)} \to \left(\hat{U}^0 + \hat{U}^{ho}\right)_{,xx} \quad \Omega_{2}^{(k)} \to \left(\hat{U}^0 + \hat{U}^{ho}\right)_{,xy} \\
&\Omega_{3}^{(k)} \to \left(\hat{U}^0 + \hat{U}^{ho}\right)_{,xz} \quad \Omega_{4}^{(k)} \to \left(\hat{U}^0 + \hat{U}^{ho}\right)_{,yy} \\
&\Omega_{5}^{(k)} \to \left(\hat{U}^0 + \hat{U}^{ho}\right)_{,yz} \quad \Omega_{6}^{(k)} \to \left(\hat{U}^0 + \hat{U}^{ho}\right)_{,zz} \\
&\Omega_{7}^{(k)} \to \left(\hat{V}^0 + \hat{V}^{ho}\right)_{,xx} \quad \Omega_{8}^{(k)} \to \left(\hat{V}^0 + \hat{V}^{ho}\right)_{,xy} \\
&\Omega_{9}^{(k)} \to \left(\hat{V}^0 + \hat{V}^{ho}\right)_{,xz} \quad \Omega_{10}^{(k)} \to \left(\hat{V}^0 + \hat{V}^{ho}\right)_{,yy} \\
&\Omega_{11}^{(k)} \to \left(\hat{V}^0 + \hat{V}^{ho}\right)_{,yz} \quad \Omega_{12}^{(k)} \to \left(\hat{V}^0 + \hat{V}^{ho}\right)_{,zz} \\
&\Omega_{13}^{(k)} \to \left(\hat{W}^0 + \hat{W}^{ho}\right)_{,xx} \quad \Omega_{14}^{(k)} \to \left(\hat{W}^0 + \hat{W}^{ho}\right)_{,xy} \\
&\Omega_{15}^{(k)} \to \left(\hat{W}^0 + \hat{W}^{ho}\right)_{,xz} \quad \Omega_{16}^{(k)} \to \left(\hat{W}^0 + \hat{W}^{ho}\right)_{,yy} \\
&\Omega_{17}^{(k)} \to \left(\hat{W}^0 + \hat{W}^{ho}\right)_{,yz} \quad \Omega_{18}^{(k)} \to \left(\hat{W}^0 + \hat{W}^{ho}\right)_{,zz}
\end{aligned} \tag{32}$$

The closed form expressions of the continuity coefficients are obtained embodying Eqs. (26) - (29) into the stress contact conditions and then solving the system with a symbolic calculus tool. To give an idea of the procedure, the solving system for a beam at the generic interface $\Im$ between the layers q and q+1 is:

$$\begin{aligned}
\Phi_x^{\Im} = &\left(Q_{44}^{+}\right)^{-1}\Bigg[\left(Q_{44}^{-} - Q_{44}^{+}\right)\Bigg(\hat{U},_z^0 + \sum_{k=1}^{q-1}\Phi_x^k + \hat{W},_x^0 + \\
&+\sum_{k=1}^{q-1}\Psi,_x^k\left(z_{\Im} - z_k\right) + \sum_{k=1}^{q-1}\Omega,_x^k\left(z_{\Im} - z_k\right)^2 + \sum_{k=1}^{q-1}C_w^k,_x\Bigg) + \\
&+Q_{44}^{-}\left(\hat{U}_q^{ho},_z + \hat{W}_q^{ho},_x\right)\Bigg] - \hat{U}_{q+1}^{ho},_z - \hat{W}_{q+1}^{ho},_x - C_w^{\Im},_x
\end{aligned} \tag{33}$$

$$\begin{aligned}
\Psi^{\Im} = &\left(Q_{33}^{+}\right)^{-1}\Bigg[\left(Q_{33}^{-} - Q_{33}^{+}\right)\Bigg(\sum_{k=1}^{q-1}\Psi^k + 2\sum_{k=1}^{q-1}\Omega^k\left(z_{\Im} - z_k\right)\Bigg) + \\
&+Q_{13}^{-}\cdot\hat{U}_q^{ho},_x + Q_{33}^{-}\cdot W_q^{ho},_z + \\
&+\left(Q_{13}^{-} - Q_{13}^{+}\right)\Bigg(\hat{U},_x^0 + \sum_{k=1}^{q-1}\Phi_x^k,_x\left(z_{\Im} - z_k\right) + \sum_{k=1}^{q-1}C_u^k,_x\Bigg) + \\
&-Q_{13}^{+}\left(\hat{U}_{q+1}^{ho},_x + C_u^{\Im},_x\right)\Bigg] - \hat{W}_{q+1}^{ho},_z
\end{aligned} \tag{34}$$

$$\begin{aligned}
\Omega^{\Im} = &\left(2Q_{33}^{+}\right)^{-1} + \Bigg[\left(Q_{13}^{-} - Q_{13}^{+}\right)\Bigg(\hat{U},_{xz}^0 + \sum_{k=1}^{q-1}\Phi_x^k,_x\Bigg) + \\
&-Q_{13}^{+}\left(\hat{U}_{q+1}^{ho},_{xz} + \Phi_x^{\Im},_x\right)\Bigg] - \frac{\hat{W}_{q+1}^{ho},_{zz}}{2}
\end{aligned} \tag{35}$$

$$\begin{aligned}
&+\left(2Q_{33}^{+}\right)^{-1}\left[Q_{13}^{-}\cdot\hat{U}_q^{ho},_{xz} + Q_{33}^{-}\cdot\hat{W}_i^{ho},_{zz}\right] + \\
&+\left(Q_{33}^{-} - Q_{33}^{+}\right)\left(Q_{33}^{+}\right)^{-1}\sum_{k=1}^{q-1}\Omega^k
\end{aligned}$$

The expressions of the continuity functions are determined at any interface between physical or computational layers by solving this system. The procedure for plates is similar, but it is here omitted for sake of brevity.

2) Hierarchic terms

The high order coefficients are here referred as hierarchic terms, since they enable a variable representation in different regions across the thickness. To obtain their expressions first of all the fulfilment of the boundary conditions prescribed by the elasticity theory across the thickness should be enforced:

$$\sigma_{xz}\,|^u = 0 \quad \sigma_{xz}|_l = 0 \tag{36}$$

$$\sigma_{yz}\,|^u = 0 \quad \sigma_{yz}|_l = 0 \tag{37}$$

$$\sigma_z\,|^u = p^0\,|^u \quad \sigma_z|_l = p^0\,|_l \tag{38}$$

$$\sigma_{z,z}\,|^u = 0 \quad \sigma_{z,z}|_l = 0 \tag{39}$$

(p^0 represents the transverse distributed loading).

In addition, it is also necessary to enforce the fulfilment of the local differential equilibrium equations:

$$\begin{aligned}
&\sigma_{x,x} + \sigma_{xy,y} + \sigma_{xz,z} = 0 \\
&\sigma_{xy,x} + \sigma_{y,y} + \sigma_{yz,z} = 0 \\
&\sigma_{xz,x} + \sigma_{yz,y} + \sigma_{z,z} = 0
\end{aligned} \tag{40}$$

at various points across the thickness. Of course, the way chosen to subdivide the structures into computational layers determines the position of these points. In fact, the number of

points where the equilibrium condition should be enforced is $n_p = N_{lay} \cdot ord\_ip - 2$, N_{lay} being the number of computational layers and *ord_ip* being the chosen order of expansion across the thickness for the in-plane displacements. The position of the n_p points is determined arbitrarily trying to fulfil the equilibrium condition (40) in all the points across the thickness of the structure, thus improving accuracy. However, the n_p points should not be placed excessively near to the interfaces, in order to avoid numerical problems (i.e. singular or badly scaled matrix).

The system of equations obtained from the fulfilment of the boundary conditions and from the enforcement of the equilibrium equations (40) at chosen points across the thickness is again solved using a symbolic calculus tool. With this approach, it is possible to easily express the hierarchic terms $\wp^{ho}$ as functions of the d.o.f., thus, on the contrary of the other models to date available it is possible to refine the solutions across the thickness without increasing the number of primary variables. For sake of clarity, hereafter, the generic expression of Eq. (40) at the point z_p for a beam is reported:

$$\begin{aligned}
&\left(Q_{13}+Q_{44}\right)\hat{W}_q^{ho},_{xz}+Q_{44}\hat{U}_q^{ho},_{zz}+Q_{11}\hat{U}_q^{ho},_{xx}= \\
&-Q_{44}\hat{U},_{zz}^{0}-Q_{11}\left(\hat{U},_{xx}^{0}+\sum_{k=1}^{q}\Phi,_{xx}^{k}\left(z_p-z_k\right)+\sum_{k=1}^{q}C_u,_{xx}^{k}\right)+ \\
&-\left(Q_{13}+Q_{44}\right)\left(\sum_{k=1}^{q}\Psi,_{x}^{k}+2\sum_{k=1}^{q}\Omega,_{x}^{k}\left(z_p-z_k\right)\right)
\end{aligned} \tag{41}$$

$$\begin{aligned}
&Q_{33}\hat{W}_q^{ho},_{zz}+Q_{44}\left(\hat{U}_q^{ho},_{zz}+\hat{W}_q^{ho},_{xz}\right)+Q_{13}\hat{U}_q^{ho},_{xz}= \\
&-Q_{13}\left(\hat{U},_{xz}^{0}+\sum_{k=1}^{q}\Phi_x,_{x}^{k}\right)-2Q_{33}\sum_{k=1}^{q}\Omega^{k}+ \\
&-Q_{44}\left(\hat{U},_{zz}^{0}+\sum_{k=1}^{q}\Psi,_{x}^{k}+2\sum_{k=1}^{q}\Omega,_{x}^{k}\left(z_p-z_k\right)\right)+
\end{aligned} \tag{42}$$

As outlined previously, by the viewpoint of the computation of the unknowns coefficients, imposing Eqs. (1) – (3) is equivalent to impose Eqs. (35) – (39). Accordingly, the high-order terms $\wp^{ho}$ appearing in the expressions (10) - (12) are also employed to fulfil the boundary conditions of Eqs. (1) to (3) at the edges of the joint.

The choice of evaluating apart once at a time in analytic form the expressions of the coefficients of displacements and of the continuity functions enables the present model to capture stress fields as accurate as 3-D models without any drawback, since its computational effort is equivalent to that of single layer models. This advantage was proven in [28], where the computational time of the model without the terms (20)-(22), here introduced in order to treat bonded joints, was compared to that of a previous model with the same number of d.o.f. and equivalent kinematic relations. This previous model had the same memory occupation, but, instead of using symbolic calculus, all the relations were obtained in approximated numerical form. Therefore, Ref. [28] showed that the drawbacks of zig-zag models can be easily overcome obtaining in an automatic way closed form expressions of high-order terms and continuity functions, thus avoiding to perform cumbersome operations and speeding-up the solution. Accordingly, this approach is also employed in the present paper.

As a general remark, it can be noticed that, even if the numerical results presented in Section 3.3 refer to reference cases taken from the literature that do not underline all the potentialities of the model, its validity is general, since it can accurately account for any stress variation.

Finally, it could be underlined that, since the stresses continuity can be enforced as boundary conditions, the representation here proposed can be also adopted to develop finite elements with different representations but with compatible stresses. Unfortunately, a direct implementation of the present structural model involves derivatives of the displacements as nodal d.o.f. To avoid this drawback, it is possible to employ the strain energy updating technique (SEUPT) by Icardi and Ferrero [30], whose features are explained in the following section.

D. Strain energy updating (SEUPT)

An SEUPT, which can be easily implemented within standard finite elements computer codes, is a procedure that can improve the results of a preliminary finite element analysis (PFEA) with standard shear deformable plate elements, using the present structural model. To summarize, spline functions interpolate the results of the PFEA in the regions of interest, then this interpolation is employed to build an updated "analytical" solution, as outlined hereafter.

Since differentiation, integration and any other operation necessary for computing the solution are performed with the spline interpolation instead of being carried out with the finite element interpolation functions, using SEUPT, no derivatives of displacements are involved as nodal d.o.f. Accordingly, the PFEA employs computationally efficient C^0 shear deformable elements with the customary displacements and shear rotations as nodal d.o.f. and efficient linear or parabolic standard interpolating functions. Of course, attention should be paid in removing reduced integration, or better, the inconsistent spurious constraints from these elements, in order to avoid shear locking.

One of the merits of SEUPT is that it enables to treat laminates with distinctly different properties of the constituent layers, strong anisotropy and loading/ boundary conditions of general interest using commercial finite element codes, whose accuracy is updated up to the level of refined AM.

In the version of SEUPT used in this paper, two sets of updating operations are separately carried out over the strain energy and over the work of external forces. Please note that, as the adaptive model here employed is able to capture the interlaminar stresses directly from the constitutive equations, the updating procedure is faster than in [30] and no derivatives of the in-plane stresses are involved.

A symbolic calculus tool is again employed to get the expressions of strain energy and of the work of external forces,

thus the energy balance is written in analytical form once at a time outside the solution process, speeding-up the computations. The following steps can be identified within the procedure.

i) First, the overall rotations $\varphi_x = \gamma_x^0 - z \cdot w^0{}_{,x}$ and $\varphi_y = \gamma_y^0 - z \cdot w^0{}_{,y}$ used as functional d.o.f. by the finite elements in the PFEA phase are made consistent with the actual structural model. To this purpose, the contributions of γ_x^0, $w^0{}_{,x}$, γ_y^0 and $w^0{}_{,y}$ are split from the spline interpolation of φ_x and φ_y. Next, the spline interpolation of $\tilde{u}^0$, $\tilde{v}^0$, $\tilde{w}^0$, $\tilde{\gamma}_x^0$ and $\tilde{\gamma}_y^0$ are introduced into the expression of the strain energy. The purpose is to compute the corrective terms $\Delta^u, \Delta^v, \Delta^w, \Delta^{\gamma_x}$ and Δ^{γ_y} that make the solution $\tilde{u}^0 + \Delta^u$, $\tilde{v}^0 + \Delta^v$, $\tilde{w}^0 + \Delta^w$, $\tilde{\gamma}_x^0 + \Delta^{\gamma_x}$, $\tilde{\gamma}_y^0 + \Delta^{\gamma_y}$ consistent with the adaptive model, simply substituting into its energy balance the expressions of the updated displacement.
A suitable choice of the set of interpolation points enables to easily overcome the ill-conditioning of the spline interpolation. As shown in Ref. **Error! Reference source not found.**, accurate results can be obtained using a 4x4 interpolation scheme around the area of interest, which determines a third-order approximation over each patch. If too many interpolation points are retained, oscillations can rise at the bounds of the sub-regions considered.

ii) The next step requires to construct the energy balance in order to evaluate the contributions $\Delta^u, \Delta^v, \Delta^w, \Delta^{\gamma_x}$ and Δ^{γ_y}. First only the correction Δ^{γ_x} is incorporated in the energy balance, assuming all the other corrections to vanish. The work of the external forces is updated in a similar way substituting the expressions of the updated displacement d.o.f. Once the first approximate Δ^{γ_x} is computed from the energy balance, it is employed to evaluate Δ^{γ_y} in a similar way postulating that all the other corrections still vanish. The solution to this and the following steps is obtained using the Penalty Function Method.

iii) Since it is expected that even the FSDPT model can quite accurately describe the membrane energy, the in-plane displacements will not vary so much applying SEUPT. However, Δ^{γ_x} and Δ^{γ_y} computed by updating the transverse shear energy, as described above, are adopted to improve the membrane energy, aiming at computing Δ^u, Δ^v and Δ^w from the energy balance. Again, each correction is assumed one by one, starting with the computation of Δ^u and assuming the remaining ones to vanish. The approximate expression of Δ^u computed by the energy balance is used to evaluate an approximate expression of Δ^v and both expressions of Δ^u are Δ^v are employed to compute Δ^w. Then the entire process is restarted and repeated till convergence after having computed the contribution by the normal stress and strain, which are disregarded by the FSDT model used in the PFEA phase, as described hereafter.

iv) The results of the PFEA provides an approximate expression of the transverse normal stress $\tilde{\sigma}_z$. In details, this stress can be recovered integrating in z the third local differential equilibrium equation (40), obtained deriving the spline representation of the transverse shear stresses in x and y. Then, using the 3D stress–strain relation, an approximate expression of the transverse normal strain $\tilde{\varepsilon}_z$ is computed. The contribution by the normal stress and strain are then substituted into the energy balance and used for computing the corrective displacements as described above.

v) The updating procedure previously described is carried out disregarding the adaptive contributions to displacements given by the hierarchic terms, and then these contributions are added and computed as outlined hereafter. After the computation in sequence of $\Delta^u, \Delta^v, \Delta^w, \Delta^{\gamma_x}, \Delta^{\gamma_y}, \tilde{\sigma}_z$ and $\tilde{\varepsilon}_z$, a sub-process is started which enforce the local equilibrium equations (40) at selected points across the thickness choosing a suitable subdivision scheme. The number of subdivision may be refined across the thickness in the regions where a higher order representation is required; however numerical tests showed that this refinement is unnecessary for undamaged laminates and sandwiches.

vi) The previous updating operations are repeated till convergence after incorporation of the hierarchic terms. The entire process which starts with the computation of Δ^{γ_x} and Δ^{γ_y} is repeated using the last correction as the entry solution for the next iteration, and the magnitude of corrective displacements as a measure of errors.

E. Solution methodology

As customarily, the Principle of Virtual work or the Rayleigh-Ritz method allow to obtain the partial differential governing equations of the present model. Their expression are rather lengthy, therefore they are here omitted for sake of brevity. Their solution is found through the Fourier series method assuming the displacement fields as:

$$u^0(x,y) = \sum_{m=1}^{M}\sum_{n=1}^{N} A_{mn} \cos\left(\frac{m\pi}{L_x}x\right)\sin\left(\frac{n\pi}{L_y}y\right) \tag{43}$$

$$v^0(x,y) = \sum_{m=1}^{M}\sum_{n=1}^{N} B_{mn} \sin\left(\frac{m\pi}{L_x}x\right)\cos\left(\frac{n\pi}{L_y}y\right) \tag{44}$$

$$w^0(x,y) = \sum_{m=1}^{M}\sum_{n=1}^{N} C_{mn} \sin\left(\frac{m\pi}{L_x}x\right)\sin\left(\frac{n\pi}{L_y}y\right) \tag{45}$$

$$\gamma_x{}^0(x,y) = \sum_{m=1}^{M}\sum_{n=1}^{N} D_{mn} \cos\left(\frac{m\pi}{L_x}x\right)\sin\left(\frac{n\pi}{L_y}y\right) \tag{46}$$

$$\gamma_y^{\,0}(x,y)=\sum_{m=1}^{M}\sum_{n=1}^{N}E_{mn}\sin\left(\frac{m\pi}{L_x}x\right)\cos\left(\frac{n\pi}{L_y}y\right) \tag{47}$$

By solving the set of algebraic equations obtained through the substitution into the governing differential equations, it is possible to get the unknown amplitudes A_{mn} to E_{mn}. Yang and Pang [27] also used this method, dividing the SLJ into three zones two of which being outside the overlap and the other being the overlap itself, but also many other researchers employed this method for solving problems with non-classical, intricate boundary conditions. Obviously, the expansion order chosen to truncate Eqs. (43) to (47) determines the computational effort. It is worthwhile to remark that that in two-dimensional problems Eqs. (44) and (46) are neglected and the solution does not vary in *y*. The applications taken from literature show that convergent results can be obtained using at least a hundred of terms, so processing time and memory occupation dimension are much larger than those required for solving problems with simple loading schemes and conventional boundary conditions.

The comparisons with analytical and finite element solutions by other researchers will show that the present model can obtain quite accurate results even using single component expansions, at least for the sample cases available in the literature, with clear advantages by the viewpoint of computational costs. In these cases, the displacements are represented as follows:

$$u^0(x,y)=A^U\left[\cosh(x)-1\right]\cos\left(\frac{\pi x}{L_x}\right) \tag{48}$$

$$w^0(x)=A^W\sin\left(\frac{\pi x}{L_x}\right) \tag{49}$$

$$\gamma_x^{\,0}(x,y)=A^{\gamma_x}\left[\cosh(x)\right]\cos\left(\frac{\pi x}{L_x}\right) \tag{50}$$

The three unknown amplitudes A^u, A^w, A^{γ_x} are determined, e.g. through minimization of the potential energy, solving a system of just three algebraic equations in three unknowns. It is underlined that, according to the reference articles used for comparisons, the variation in the *y* direction is neglected.

III. Numerical Applications and Discussion

The capabilities of the present model were already proven in Refs. [28] and [29], where applications to laminates and sandwiches were presented keeping fixed the in-plane representation. Here the aim is to verify whether the displacement-based structural model, the displacement fields and the solution approach explained above can be efficiently employed for the analysis of adhesively bonded joints.

To this purpose, sample cases of SLJ and DLJ taken from the literature are analysed using the present model.

Aiming at assessing the capability of the present analytical model to treat general boundary conditions, which is a requirement of primary importance at the edges of the overlap, the analysis of a plate with clamped edges is premised to the analysis of joints. While in order to assess the accuracy and the efficiency of the present model in predicting the distribution of out-of-plane stresses across the thickness of the adhesive film, the analysis of a piezoactuated beam made of an aluminium substrate, a bonding film and a piezoactuator is also premised.

All the computational times provided in the following sections are obtained performing the analyses on a laptop computer with dual-core CPU 2.20 GHz, 64 bit operating system and 4 GB RAM.

A. Plate with clamped edges

Customarily, the researchers employ benchmark solutions for simply supported laminates and sandwiches to assess the accuracy of their plate theories and finite element formulations, not considering clamped or free edges. This choice prevents from verifying whether the behaviour of the models with mid-plane displacements and shear rotations as functional d.o.f., like the present model, can be poor. In fact, this kind of models is not always capable to enforce at the clamped edge a non-vanishing transverse shear with displacements and shear rotations that vanish. Aiming at verifying the capability of the present model to deal with general boundary conditions, here the square plate analysed by Vel and Batra in Ref. [31] is considered.

The plate, characterized by a length to thickness ratio (L_x/h) of 5, is simply supported on two opposite edges, clamped on the other two and it is undergoing a bi-sinusoidal normal load with intensity p^0 on the upper face, whereas the bottom one is traction free. The material constituting the plate has the following mechanical properties: $E_L/E_T=25$; $G_{LT}/E_T=0.5$; $G_{TT}/E_T=0.2$; $\upsilon_{LT}=0.25$, while the stacking sequence is [0°/90°/0°]. The present model carries out the analysis considering the following in-plane representation of the d.o.f.:

$$u^0(x,y)=\sum_{m=2,4}^{M}\sum_{n=1,3}^{N}A_{mn}\sin\left(\frac{m\pi}{L_x}x\right)\cos\left(\frac{n\pi}{L_y}y\right) \tag{51}$$

$$v^0(x,y)=\sum_{m=1,3}^{M}\sum_{n=2,4}^{N}B_{mn}\cos\left(\frac{m\pi}{L_x}x\right)\sin\left(\frac{n\pi}{L_y}y\right) \tag{52}$$

$$w^0(x,y)=\sum_{m=2,4}^{M}\sum_{n=2,4}^{N}C_{mn}\left[\cos\left(\frac{m\pi}{L_x}x\right)-(-1)^{m/2}\right]\left[\cos\left(\frac{n\pi}{L_y}y\right)-(-1)^{n/2}\right] \tag{53}$$

$$\gamma_x^0(x,y)=\sum_{m=2,4}^{M}\sum_{n=1,3}^{N}D_{mn}\sin\left(\frac{m\pi}{L_x}x\right)\cos\left(\frac{n\pi}{L_y}y\right) \tag{54}$$

$$\gamma_y^0(x,y) = \sum_{m=1,3}^{M} \sum_{n=2,4}^{N} E_{mn} \cos\left(\frac{m\pi}{L_x} x\right) \sin\left(\frac{n\pi}{L_y} y\right) \qquad (55)$$

As far as the through-the-thickness representation is concerned, the adaptive model employs three computational layers, while the points where the equilibrium condition (40) is enforced are [-0.43h; -0.22h; -0.14h; 0; 0.09h; 0.23h; 0.44h].
Vel and Batra [31] exactly solved the governing equations using a three-dimensional generalization of the Eshelby-Stroh formalism that determines an infinite system of equations in infinite unknowns. Using the boundary conditions at the edges and the continuity conditions at the interfaces, they defined constants in the general solution, which were determined by the Fourier series method. Truncations of the set of infinite equations introduce errors that decrease by increasing the number of the terms in the series.

Table 1 reports the through-the-thickness variations of the transverse shear stress and of the transverse displacement predicted by the present model and by Vel and Batra [31] with 250 terms in the series. Please note that, the results in Table I named 'Present M, N=200' are obtained considering 200 terms in Eqs. (51) – (55), while the ones named 'Present M, N=1' are computed considering just a single component in the series expansion, i.e. M=N=1.
The results of Table I are normalized as follows according to [31]:

$$\bar{\sigma}_{xz} = \frac{10 \cdot H \cdot \sigma_{xz}\left(\frac{L_x}{8}, \frac{L_y}{2}, z\right)}{p^0 L_x} \qquad (56)$$

$$\bar{w} = \frac{100 E_T \cdot h^3}{p^0 L_x^4} w(0,0,z)$$

From the results of Table I, it could be seen that the through-the-thickness variation of solutions predicted by the present model is in good agreement with the reference results even when just a one terms representation is considered, thus reducing to the minimum the computational burden. This achievement is reached thanks to the *a priori* fulfilment of the stress and displacement boundary conditions and of the interfacial stress contact conditions, obtained with the computation of closed form expressions for the coefficients of displacements. The evaluation of these coefficients, which is required just once at a time, takes about a minute, while the solution of the governing equations takes four minutes with M=N=200 and 1.3 s with M=N=1. So, it could be noticed the capability of the model of being accurate with a low expansion order, which gives a considerable practical advantage when repeated computations are required.

B. Piezoelectrically actuated beam

As a further assessment of the model, its capability to predict the stress across the thickness of the adhesive is tested. To this purpose, a three layered cantilever beam made of an underlying aluminium beam substructure, an adhesive film and a piezoactuator bonded on the upper face is considered. The analysis of piezoactuated structure is a subject largely studied by the researchers, as shown by Refs. [32] - **Error! Reference source not found.**. Here the case considered by Robbins and Reddy [32] is analysed. Similarly to what happens for bonded joints, close to the free edge of the beam the transverse normal and shear stresses reach a very large peak nearly in the adhesive layer. As a consequence of these interlaminar stress concentrations, the adhesive layer may progressively fail till to complete debonding of the piezoactuator. Robbins and Reddy studied this case employing finite elements deriving from a displacement-based layerwise theory and their result showed that unwanted dangerous stress concentrations occur at the free edge, thus increasing the possibility of a debonding of the piezoactuator in service.

We choose to consider this sample case because its stress field is similar to those of bonded joints and also because Robbins and Reddy presented the stress distributions across the thickness in the most critical regions. Thus it is possible to verify the accuracy of the present model not just considering the in-plane stress distributions. In fact, for what concerns the analysis of joints, generally the results across the thickness are not provided by the researchers, because the analyses are carried out postulating simplifying assumptions, such as a constant transverse shear stress across the thickness of the adhesive layer. The main goal here is to investigate the effectiveness of the present model at the light of the localized effects due to the piezoactuator control layers on the through-the-thickness stress distribution across the adhesive layer.

The materials constituting the beam have the following mechanical properties: aluminium E= 69 GPa, G=27.5 GPa, υ=0.25; adhesive: E= 6.9 GPa, G=2.5 GPa, υ=0.4; piezoactuator: E_1= 69 GPa, E_3= 48 GPa, G=21 GPa, υ_{13}= 0.25, υ_{13}= 0.175. The beam is 152 mm long, the aluminium substrate is 15.2 mm thick, while the thicknesses of the adhesive layer and of the piezoactuator are respectively 0.254 mm and 1.52 mm. The only acting loads are the self-equilibrating loads induced by the piezoactuator. A bending deformation is provided by applying an actuation strain of 0.001 to the piezoelectric layer via an applied electric field.

Table II shows the through-the thickness distribution of membrane, transverse shear and transverse normal stresses close to the free edge, while Table III reports the in-plane variation of the stress field near the top of the aluminium substrate (z= 6.61 mm) and in the piezoelectric layer (z= 6.6245 mm). According to [32], the stress distributions are normalized as follows:

$$\bar{\sigma}_{xx} = \frac{A_{tot} \cdot \sigma_{xx} \cdot 10^{3}}{(E_1 A)_{alum} + (E_1 A)_{ad} + (E_1 A)_{piezo}}$$
$$\bar{\sigma}_{zz} = \frac{A_{tot} \cdot \sigma_{zz} \cdot 10^{3}}{(E_3 A)_{alum} + (E_3 A)_{ad} + (E_3 A)_{piezo}} \quad (57)$$
$$\bar{\sigma}_{xz} = \frac{A_{tot} \cdot \sigma_{xz} \cdot 10^{3}}{(G_{13} A)_{alum} + (G_{13} A)_{ad} + (G_{13} A)_{piezo}}$$

Where the subscripts *alum*, *ad*, *piezo* and *tot* indicate the cross sectional area and the elastic moduli of the substrate structure, of the adhesive and of the piezoactuator layer, respectively.

In this case, the adaptive model carries out the analysis considering 6 subdivisions across the thickness of the aluminium substrate, 5 subdivisions the adhesive layer and 9 in the piezoactuator layer. In order to improve accuracy, these computational layers are refined near the adhesive layer and gradually enlarged as the distance to this layer increases.

Hermite's cubic polynomials are used for all the functional d.o.f. far from the tip and the root of the beam:

$$C_1 H_1(x) + C_2 H_2(x) + C_3 H_3(x) + C_4 H_4(x) \quad (58)$$

Instead, at the tip and the root of the beam the trial functions are chosen as follows in order to fulfil the boundary conditions, i.e. $w(0)= w_{,x}(0)= 0$ and $\int z\sigma_{xx} dz = 0$:

$$w^0(x) = \left[1-(i+3)\frac{x}{L} - \left(1-\frac{x}{L}\right)^{i+3} \right] A^w \quad (59)$$

Where i=1. Please note that the in-plane displacement and the shear rotation are obtained from (59) deriving in x and considering A^u and A^{γ_x} as amplitudes.

The boundary conditions at the points where the representation is changed and the condition $\int z\sigma_{xz} dz = 0$ are imposed as outlined in Section 2.3.2.

Also in this case, the results by the present model are in accordance with the reference ones and the boundary conditions are correctly fulfilled. As far as the computational burden is concerned, even if many subdivisions are considered across the thickness and several are used in the spanwise direction, just 150 s are required to perform the analysis. Accordingly, the results for this sample case demonstrate that the present model can couple accuracy and efficiency.

C. Adhesively bonded joints

In order to test the capability of the present model to deal with joints, the sample cases by Radice and Vinson [7], Andruet et al. [8], Diaz [10] and Nemes and Lachaud [12] are considered.

1) Case A: single-lap joint with aluminum adherents

The first case takes into consideration the single lap joint analysed by Radice and Vinson [7]. The joint is clamped at the left edge and simply supported at the right one, where an axial load with intensity 40 kN/mm is applied. The adherents are made of aluminium (E=70 GPa, υ=0.33), while the adhesive is an epoxy resin, here, according to [7], treated as an isotropic material (E=4.82 GPa, υ=0.40). The adherents are 50.8 mm long and 1.62 mm thick, while the length of the adhesive is 12.7 mm and its thickness is 0.25 mm. According to [7], the variation of solutions in the transverse direction y is not considered.

In Figure 2 two results by the present model are reported: those named 'Present M,N=1' are computed using as trial functions in the overlap those of Eqs. (48)- (50) with a single component, while the results named 'Present M,N=30' are obtained using in the overlap the trial functions of Eqs. (43) - (47) with 30 components. In the former case, the problem is reduced to solving a system of 3 equations in 3 unknowns, therefore the analysis is consistently speeded-up as it takes only 1.5 s. Instead, with the latter approach the solving system is a 90 x 90 and the computational time is 80 s. In both cases, aiming at fulfilling the boundary conditions, the trial functions of Eqs. (51) – (55) are chosen in the lower adherent, while those of Eqs. (43) – (47) are employed into the upper adherent. Irrespectively of the trial functions adopted, the adaptive model adopts a third order expansion of the in-plane displacement and a fourth order expansion of the transverse displacement. The equilibrium condition (40) for computing the hierarchic terms of the adaptive model is imposed at the following through-the-thickness points [-1.2; -0.67; -0.063; -0.015; 0.063; 0.67; 1.2].

In order to assess the effectiveness of SEUPT in analysing joints, in Figure 2 are also reported the results computed with this procedure (i.e. the curves named 'SEUPT'). Specifically the PFEA is carried out using a model considering 1000 d.o.f. and then these preliminary results are post-processed with SEUPT. As shown by the numerical results, also this latter approach provides accurate results, while the computational time required for the application of the procedure is 96 s.

It could be noticed that the comparison with the reference case confirms the accuracy of the model even when just a single component in the series expansion of the trial functions is considered.

2) Case B: single-lap joint with aluminum adherents

We now focus our attention on the single lap joint analysed by Andruet et al. [8] with aluminium adherents 60 mm long and 1.6 mm thick. The adhesive is an epoxy resin, its thickness is 0.1 mm and the overlap length is 20 mm. The joint is clamped at left edge and simply supported at the right one. The mechanical properties of the adherents are E=68.3 GPa, υ=0.3, those of the adhesive are E=2.5 GPa, υ=0.3.

In Figure 3 two results obtained with the adaptive model are reported: that named as BC1 is computed imposing the constraints prescribed by the theory of elasticity, that named BC2 is instead obtained imposing the same value as Andruet et al. [8] of the shear stress at the edge of the joint.

In both cases, the through-the-thickness variation of the in-plane displacement is of third order and that of the transverse displacement is of fourth order, while the trial functions are

those of Eqs. (51) – (55) for the adherents and those of Eqs. (48) - (50) for the overlap. Irrespectively of the constraints imposed, the analysis takes 1.5 s. As far as the computation of the higher order terms is concerned, the equilibrium condition (40) is imposed at the following through-the-thickness points [-1; -0.5; -0.04; +0.0125; 0.04; 0.52; 1.1].

Also in this case the present model provides results as accurate as those of the reference case, even if the computational effort is very low.

3) Case C: single-lap joint with composite adherents

As a further assessment we now consider the single lap joint studied by Diaz et al. [10]. The joint has laminated graphite/epoxy (XAS/914C) adherents, whose mechanical properties are: E_x= 138 GPa, E_y= E_z= 9.4 GPa, υ_{xy}= υ_{xz}= υ_{yz}= 0.32, G_{xy}= G_{xz}= G_{yz}= 6.70 GPa. The stacking sequence is $[0° / 45° / -45° / 0°]_{2s}$, the length of the adherents is 114.3 mm, their thickness is 2 mm. The adhesive, according to [10] here treated as isotropic material, is epoxy resin REDUX 308A, with the following mechanical properties: E= 3 GPa, υ= 0.31, G= 1.15 GPa. The adhesive layer is 0.13 mm thick and the overlap length *ol* is 25.4 mm. The right edge of the joint is clamped, while the left one has all the displacements and rotations restricted except the in-plane displacement along x. A traction load with intensity P=4448 N is applied at the end cross section of the lower adherent.

Please note that in Figure 4 the stresses (y axes) are reported normalized with respect to the applied load P, while the in-plane coordinate (x axis) is normalized with respect to the overlap length *ol*.

As in Case B, in Figure 4 are reported two results obtained with the adaptive model. Those referred as BC1 are achieved imposing the constraints of Eqs. (1) – (3), instead, those named as BC2 are computed imposing the same value as Diaz et al. [10] of the shear stress at the edge of the overlap.

Irrespectively of the constraints imposed, the trial functions are those of Eqs. (51) – (55) for the adherents and those of Eqs. (48) - (50) in the overlap, and, as previously done, the through-the-thickness representation of the in-plane displacement is computed using a third order expansion, that of the transverse displacement is obtained with a fourth order expansion. Within the adherents four computational layers are considered, while a single computational layer is considered in the overlap. With this choice it is possible to improve accuracy, as the equilibrium condition (40) is imposed in an increased number of points. Specifically this condition is enforced at the following through-the-thickness points [-1.965; -1.665; -1.465; -1.365; -1.165; -0.965; -0.815; -0.665; -0.465; -0.365; -0.265; -0.05; 0.01; 0.055; 0.265; 0.365; 0.465; 0.665; 0.815; 0.965; 1.165; 1.365; 1.465; 1.665; 1.965]. As far as the computational burden is concerned, the analysis takes 1.7 s irrespectively of the boundary conditions imposed, while the results by Diaz et al. [10] takes hours for running on a computer with two quad-core CPU 2.3 GHz and 32 GB RAM.

Similarly to what done for Case A, in order to prove the qualities of SEUPT when analyzing laminates, in Figure 4 the results obtained applying this procedure are reported and named 'SEUPT'. The results of the PFEA are obtained with a model that has 1500 d.o.f.

Also in this case the comparison with the reference results proves that the present model can get accurate results, keeping very low the computational effort, even when the adherents are made of orthotropic materials. For what concerns SEUPT, also in this case, this technique gives precise results requiring a computational time of 115 s.

4) Case D: double-lap with aluminium adherents

We now focus our attention on the analysis of double lap joints. While SLJ undergo a large transverse displacement, the symmetry of DLJ hinders this effect. We now consider the joint with aluminium 2024 T3 adherents analysed by Nemes and Lachaud [12]. The adhesive is epoxy resin REDUX 312/5 (E=27 GPa, G=1 GPa, υ=0.35) and it is 0.1 mm thick. The thickness of the outer adherents is 2 mm, that of the inner adherent is 4 mm and the overlap length is 50 mm. The lower and the upper adherents are clamped, while a pressure load with intensity 1 N/mm is applied to the inner adherent.

As in Case A, in Figure 5 two results by the present model are reported: those named 'Present M,N=1', and those named 'Present M,N=30'. In the former case the analysis is carried out using in the overlap the trial functions of Eqs. (48)- (50) with a single component, thus the problem is reduced to the solution of a system of 3 equations in 3 unknowns. In the latter case the computations are performed using in the overlap the trial functions of Eqs. (43) - (47) with 30 components. As a consequence the solving system is a 90 x 90. Of course, the first approach is dramatically more efficient than the second one, as it takes only 1.65 s instead of 90 s. Irrespectively of the trial functions chosen within the overlap, the in-plane representation adopted in the outer adherents is that of Eqs. (51) – (55), while in the inner adherent the trial functions are those of Eqs. (43) – (47). As far as the through-the-thickness representation is concerned, in both cases a third order expansion of the in-plane displacement and a fourth order expansion of the transverse displacement are adopted, while a single computational layer is considered in the adherents as well as in the adhesive. It could be noticed that the equilibrium condition (40) for computing the hierarchic terms of the adaptive model are imposed at the following through-the-thickness points [-2.5; -1.5; -1.07; -1.04; -1.03; -0.7; -0.1; 0.7; 1.03; 1.04; 1.07; 1.5; 2.5].

It can be seen that also in case of DLJ the approach presented in this paper still provides accurate results with low computational effort.

As general remarks about the numerical results presented, it is underlined that the model here proposed always obtains accurate results with a low computational effort. Even if just two-dimensional results were presented, since the variation in the transverse direction *y* was neglected by the analytical models used as reference cases the numerical results of Section 3.1 and of Ref. [28] and [29] prove that the present model can correctly perform full three-dimensional analyses. As outlined in Refs.[28] and [29], the adaptive model was developed in order to treat thick structures, while the sample cases here

considered refer to joints with adherents characterized by a high length to thickness ratio, because only such results are available in the literature. Accordingly its inherent numerical efficiency will be more evident analysing thick bonded joints with abruptly changing material properties of the constituent layers and distinctly different properties of the adherents, since these structures need extremely refined finite element models. It is reminded that in such cases the customary assumptions of simplified models can be no longer valid, due to intricate out-of-plane stress fields.

IV. Concluding remarks

A zig-zag model with variable kinematics was refined for the analysis of adhesively bonded joints with laminated adherents, thus allowing treating laminates and bonded joints under a unified approach. Its three-dimensional, piecewise displacement field *a priori* fulfils the stress boundary conditions at the upper and lower faces of the structure and the out-of-plane stress contact conditions at the interfaces of adjacent layers.

Aiming at better modelling the variation of solutions and at satisfying the stress boundary conditions of the joint, the in-plane representation can change from the adherents to the overlap. While thanks to a variable through-the-thickness representation, the model can accurately describe the stress field of structures with abruptly changing materials' properties. Despite a variable representation can be obtained, no increase of the memory storage dimension and no consistent increase of the processing time are required, because the model has five functional d.o.f., like classical plate models. Using symbolic calculus, closed form expressions of high-order terms and continuity functions are obtained enforcing the continuity of out-of-plane stresses at the interfaces of adjacent layers and the boundary conditions prescribed by the elasticity theory. The structural model here proposed can be also adopted to develop finite elements with different representations but with compatible stresses. However, its direct implementation would be unpractical, since derivatives of the displacements should be chosen as nodal d.o.f. To avoid this drawback, in the present paper it was suggested the implementation of the strain energy updating technique (SEUPT [30]), which is a post processing procedure able to improve the accuracy of standard finite elements up to that of refined structural model.

As a preliminary assessment, a plate with clamped edges was analysed, in order to show the capability of the present analytical model to treat general boundary conditions, like at the edges of the overlap. A piezoactuated beam made of an aluminium substrate, a bonding film and a piezoactuator was also considered in order to assess whether the present model can capture the out-of-plane stress fields across the thickness of the adhesive. For both benchmark cases, accurate results were obtained, as shown by the comparison with the reference three-dimensional results in the literature, in few seconds.

Applications to single and double-lap joints taken from the literature were presented, in order to assess the potentialities of the model. These sample cases, which have isotropic or laminated adherents, were solved through Fourier's series expansion, but accurate results were obtained even using just one component in all the examined cases. In two cases, also the results computed applying SEUPT were presented, showing that this procedure represents a valid alternative to the direct application of the model.

The numerical results showed that the current particularized version of the model with also in-plane variable kinematics can accurately and efficiently treat bonded joints with laminated adherents. In fact, for all the examined cases, accurate results were obtained in few seconds performing the analyses on a laptop computer.

References

[1] S.C. Her, "Stress analysis of adhesively-bonded lap joints", *Comp. Struct.*, vol. 47, pp. 673-678, 1999.

[2] J.R. Vinson, "Adhesive bonding of polymer composites", *Polym. Eng. Sci.*, vol. 29, pp. 1325-1331, 1989.

[3] X. He, "A review of finite element analysis of adhesively bonded joints", *Int. J. of Adhesion and Adhesives*, vol. 31, pp. 248-264, 2011.

[4] L.F.M. da Silva, P.J.C. das Neves, R.D. Adams, J.K. Spelt, "Analytical models of adhesively bonded joints-part II: comparative study", *Int. J. of Adhesion and Adhesives*, vol. 29, pp. 331-341, 2009.

[5] P.A. Gustafson, A. Bizard, A.M. Waas, "Dimensionless parameters in symmetric double lap joints: an orthotropic solution for thermo-mechanical loading", *Int. J. Solids Struct.*, vol. 44, pp. 5774–95, 2007.

[6] S.A. Yousefsani, M. Tahani, "Accurate determination of stress distributions in adhesively bonded homogeneous and heterogeneous double-lap joints", *European Journal of Mechanics – A/Solids*, vol. 39, pp. 197-208, 2013.

[7] J.J. Radice, J.R. Vinson, "On the analysis of adhesively bonded structures: a higher order semi-elastic adhesive layer model", *Comp. Sci. Tech.*, vol. 68, pp. 376-386, 2008.

[8] R.H. Andruet, D.A. Dillard, S.M. Holzer, "Two- and three-dimensional geometrical nonlinear finite elements for analysis of adhesive joints", *Int. J. of Adhesion and Adhesives*, vol. 21, pp. 17-34, 2001.

[9] I.T. Pearson, J.T. Mottram, "A finite element modelling methodology for the non-linear stiffness evaluation of adhesively bonded single lap-joints: Part 1. Evaluation of key parameters", *Comput. & Struct.*, vol. 90 – 91, pp. 76-88, 2012.

[10] J. Diaz, L. Romera, S. Hernàndez, A. Baldomir, "Benchmarking of three-dimensional finite element models of CFRP single-lap bonded joints", *Int. J. of Adhesion and Adhesives*, vol. 30, pp. 178-189, 2010.

[11] W. Xu, G. Li, "Finite difference three-dimensional solution of stresses in adhesively bonded composite tubular joints subjected to torsion", *Int. J. of Adhesion and Adhesives*, vol. 30, pp. 191-199, 2010.

[12] O. Nemes, F. Lachaud, "Double-lap adhesive bonded-joints assemblies modeling", *Int. J. of Adhesion and Adhesives*, vol. 30, pp. 288-297, 2010.

[13] O. Sayman, V. Arikan, A. Dogan, I.F. Soykok, T. Dogan, "Failure analysis of adhesively bonded composite joints under transverse impact and different temperatures", *Comp. Part B*, vol. 54, pp. 409-414, 2013.

[14] T.U. Kim, "The J-integral for single-lap joint using the stress field from the mixed variational principle", *Acta Mechanica*, to be published, doi: 10.1007/s00707-013-0882-6.

[15] L.F.M. da Silva, R.D. Adams, "Adhesive joints at high and low temperatures using similar and dissimilar adherends and dual adhesives", *Int. J. of Adhesion and Adhesives*, vol. 27, pp. 227-235, 2007.

[16] M. Quaresimin, M. Ricotta, "Fatigue behaviour and damage evolution of single-lap bonded joints in composite material", *Comp. Sci. Tech.*, vol. 66, pp. 176-187, 2006.

[17] O. Volkersen, "Die nietkraftverteilung in zugbeanspruchten nietverbindungen mit konstanten laschenquerschnitten", *Luftfahrtforschung*, vol. 35, pp. 4–47, 1938.

[18] M. Goland, E. Reissner, "The stresses in cemented joints", *Journal of Applied Mechanics*, vol. A1, pp. 17-27, 1944.
[19] L.J. Hart-Smith, "Adhesive-bonded single-lap joints", Technical report NASA CR 112236, 1973.
[20] S. Kapuria, J.K. Nath, "On the accuracy of recent global-local theories for bending and vibration of laminated plates", *Comp. Struct.*, vol. 95, pp. 163 – 172, 2013.
[21] W.J. Renton, J.R. Vinson, "The efficient design of adhesive bonded joints", *Int. J. of Adhesion*, vol. 7, pp. 175-193, 1975.
[22] S. Srinivas, "Analysis of bonded joints", NASA Technical Note TN D-7855, 1975.
[23] D.J. Allman, "A theory for elastic stresses in adhesive bonded lap joints", *Quart. J. Mech. & Appl. Math.*, vol. 30, pp. 415-436, 1977.
[24] R.D. Adams, V. Mallick, "A method for the stress analysis of lap joints", *Int. J. Adhesion*, vol. 38, pp. 199- 217, 1992.
[25] F. Mortensen, O.T. Thomsen, "Analysis of adhesive bonded joints: a unified approach", *Comp. Sci. & Tech.*, vol. 62, pp. 1011 – 1031, 2002.
[26] G.P. Zou, K. Shahin, F. Taheri, "An analytical solution for the analysis of symmetric composite adhesively bonded joints", *Comp. Struct.*, vol. 65, pp. 499 – 510, 2004.
[27] C. Yang, S.S. Pang, "Stress analysis of single-lap composite joints under tension", *ASME J. Eng. Mater. Technol.*, vol. 118, pp. 247-255, 1996.
[28] U. Icardi, F. Sola, "Development of an efficient zig-zag model with variable representation of displacements across the thickness", J. Eng. Mech. , to be published, doi: 10.1061/(ASCE)EM.1943-7889.0000673.
[29] U. Icardi, F. Sola, "Recovering critical stresses in sandwiches using through-the-thickness reinforcement", *Comp. Part B*, vol. 54, pp. 269-277, 2013.
[30] U. Icardi, L. Ferrero, "Impact analysis of sandwich composites based on a refined plate element with strain energy updating", *Comp. Struct.*, vol. 89, pp. 35-51, 2009.
[31] S.S. Vel, R.C. Batra, "Analytical solution for rectangular thick laminated plates subjected to arbitrary boundary conditions", *AIAA J.*, vol. 11, pp. 1464-1473, 1999.
[32] D.H. Robbins, J.N. Reddy, "Analysis of piezoelectrically actuated beams using a layerwise displacement theory", *Comput. & Struct.*, vol. 11, pp. 265-279, 1991.
[33] K.E. Molyet, "Study of induced strain transfer in piezoceramic smart material systems", *Smart Mater. Struct.*, vol. 8, pp. 672–690, 1999.
[34] X.D. Wang, S.A. Meguid, "On the electroelastic behaviour of a thin piezoelectric actuator attached to an infinite host structure", *Int. J. Solids Struct.*, vol. 37, pp. 3231–3251, 2000.
[35] B.N. Zhang, J.Q. Zhang, "A sub-layer model for a thick piezoelectric patch bonded on elastic substrate", *Acta Mechanica*, vol. 170, pp. 163-186, 2004.
[36] S. Kapuria, J.K. Nath, "Coupled global-local and zigzag-local laminate theories for dynamic analysis of piezoelectric laminated plates", J. of Sound and Vibration, vol. 332, pp. 306-325, 2013.

TABLE I
COMPARISON BETWEEN THE THROUGH-THE-THICKNESS DISTRIBUTIONS OF SHEAR STRESS AND TRANSVERSE DISPLACEMENT BY THE PRESENT MODEL AND BY VEL AND BATRA [31].

	z/h	-0.50	-0.40	-0.30	-0.20	-0.10	0.00	0.10	0.20	0.30	0.40	0.50
$\bar{\sigma}_{xz}$	Present M, N=1	0.000	2.610	3.230	2.641	2.110	2.096	2.100	2.270	3.343	2.733	0.000
	Present M, N=200	0.000	2.608	3.227	2.643	2.114	2.094	2.099	2.668	3.340	2.735	0.000
	Ref. [31]	0.000	2.609	3.227	2.643	2.113	2.093	2.100	2.668	3.340	2.734	0.000
$\bar{w}$	Present M, N=1	1.151	1.157	1.159	1.165	1.170	1.181	1.188	1.199	1.210	1.215	1.224
	Present M, N=200	1.153	1.158	1.161	1.168	1172	1.180	1.188	1.197	1.207	1.217	1.228
	Ref. [31]	1.152	1.158	1.162	1.167	1.173	1.180	1.188	1.198	1.208	1.218	1.227

TABLE II
COMPARISON BETWEEN THE THROUGH-THE-THICKNESS DISTRIBUTIONS OF IN-PLANE. SHEAR AND TRANSVERSE NORMAL STRESSES BY THE PRESENT MODEL AND BY ROBBINS AND REDDY [32].

	z/h	-0.50	-0.30	-0.10	0.16	0.25	0.33	0.37	0.38	0.39	0.45	0.50
$\bar{\sigma}_{xx}$	Present	0.0000	0.0006	-0.0010	0.0006	0.0088	0.0334	0.1943	0.3536	0.1664	-0.0552	0.0000
	Ref. [32]	0.0000	0.0006	-0.0010	0.0006	0.0087	0.0340	0.1950	0.3530	0.1666	-0.0551	0.0000
$\bar{\sigma}_{xz}$	Present	0.0000	-0.0191	-0.0404	-0.0487	-0.0404	0.0416	0.3799	0.4110	0.4701	0.0564	0.0000
	Ref. [32]	0.0000	-0.0190	-0.0408	-0.4930	-0.0400	0.0418	0.3798	0.4111	0.4699	0.0559	0.0000
$\bar{\sigma}_{zz}$	Present	0.0000	-0.0257	-0.0930	-0.2128	-0.2424	-0.1866	-0.1554	-0.1193	-0.0897	-0.0585	0.0000
	Ref. [32]	0.0000	-0.0276	-0.0907	-0.2129	-0.2425	-0.1863	-0.1545	-0.1192	-0.0897	-0.0590	0.0000

TABLE III.
COMPARISON BETWEEN THE IN-PLANE DISTRIBUTIONS OF IN-PLANE. SHEAR AND TRANSVERSE NORMAL STRESSES BY THE PRESENT MODEL AND BY ROBBINS AND REDDY [32].

		x	0.840	0.900	0.910	0.925	0.946	0.958	0.973	0.985	0.995	1.000
$\overline{\sigma}_{xx}$	z= 6.61 mm	Present	0.2921	0.2921	0.2943	0.2985	0.3113	0.3197	0.3261	0.2921	0.2178	0.0000
		Ref.[32]	0.2921	0.2921	0.2944	0.2990	0.3115	0.3201	0.3563	0.2921	0.2178	0.0000
	z= 6.6245 mm	Present	0.0292	0.0306	0.0319	0.0325	0.0403	0.0444	0.0556	0.0500	0.0319	0.0000
		Ref.[32]	0.0292	0.0306	0.0320	0.0326	0.0400	0.0445	0.0556	0.0501	0.0318	0.0000
$\overline{\sigma}_{xz}$	z= 6.61 mm	Present	0.0000	0.0179	0.0285	0.0540	0.1219	0.1644	0.2514	0.3257	0.3448	0.0000
		Ref.[32]	0.0000	0.0180	0.0285	0.0545	0.1220	0.1650	0.2517	0.3260	0.3450	0.0000
	z= 6.6245 mm	Present	0.0000	0.0321	0.0422	0.0740	0.1401	0.1861	0.2879	0.3381	0.4320	0.0000
		Ref.[32]	0.0000	0.0320	0.0420	0.0740	0.1400	0.1860	0.2880	0.3380	0.4320	0.0000
$\overline{\sigma}_{zz}$	z= 6.61 mm	Present	0.0000	0.0045	0.0045	0.0065	0.0146	0.0247	0.0348	0.0045	-0.0803	-0.5000
		Ref.[32]	0.0000	0.0044	0.0045	0.0660	0.0148	0.0250	0.0345	0.0046	-0.0800	-0.5000
	z= 6.6245 mm	Present	0.0000	0.0020	0.0041	0.0060	0.0100	0.0140	0.0280	0.0156	-0.0795	-0.1806
		Ref.[32]	0.0000	0.0020	0.0040	0.0060	0.0099	0.0139	0.0278	0.0159	-0.0794	-0.1806

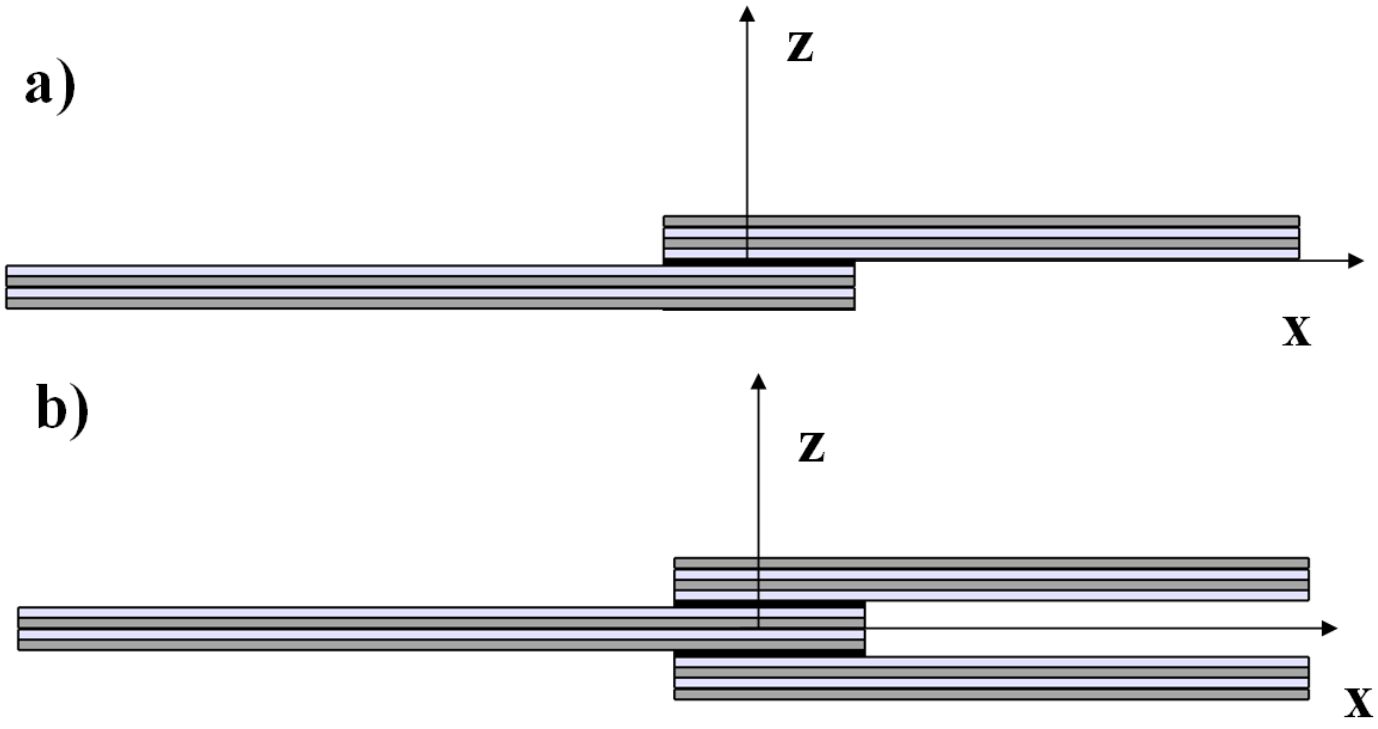

Fig. 1. Geometry and system of reference for analysis of single lap and double lap joints.

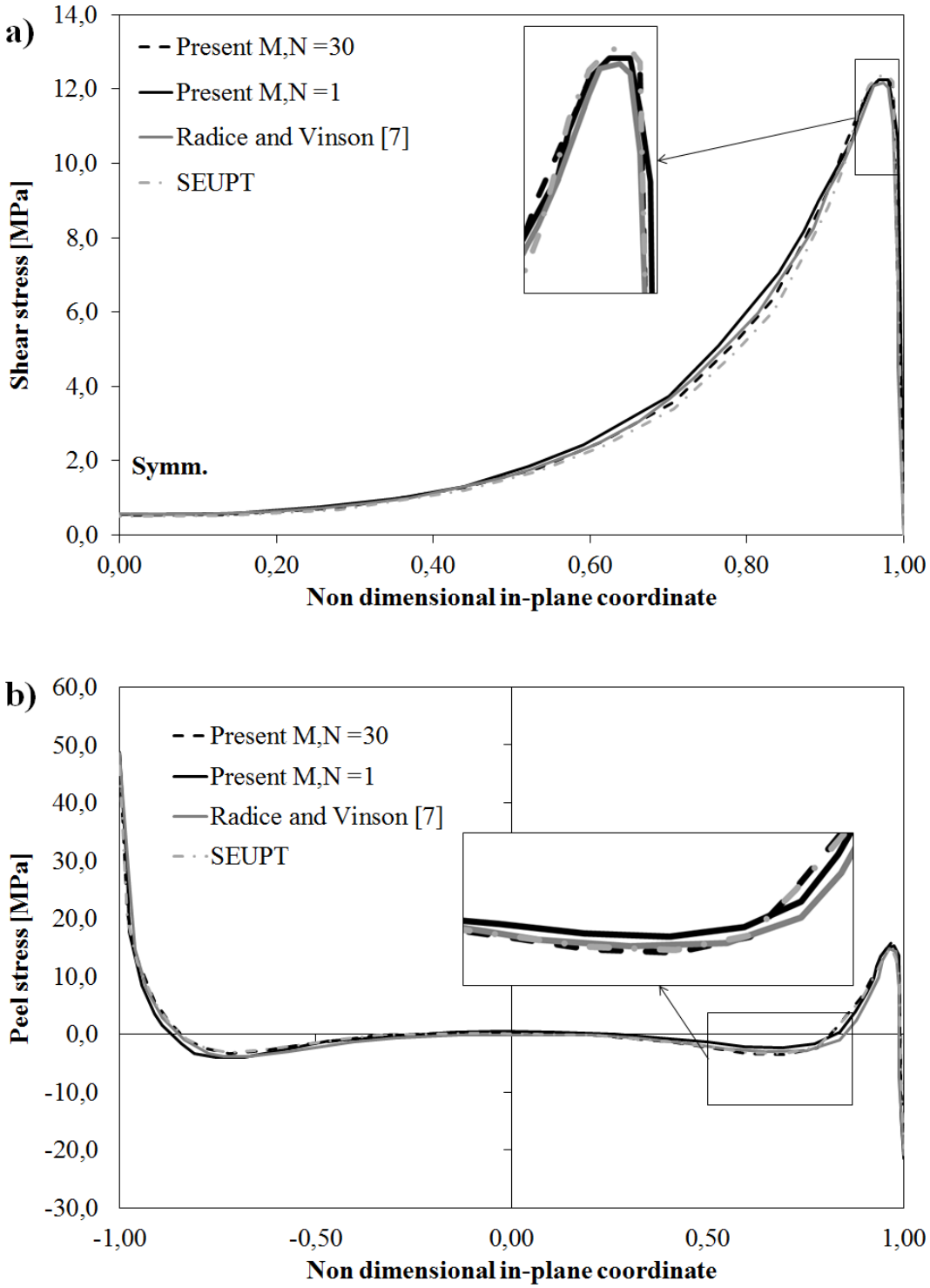

Fig. 2. Span-wise distribution of a) shear stress and b) peel stress at the interface between adhesive and adherent by Radice and Vinson [7], by the present model using different trial functions and using SEUPT.

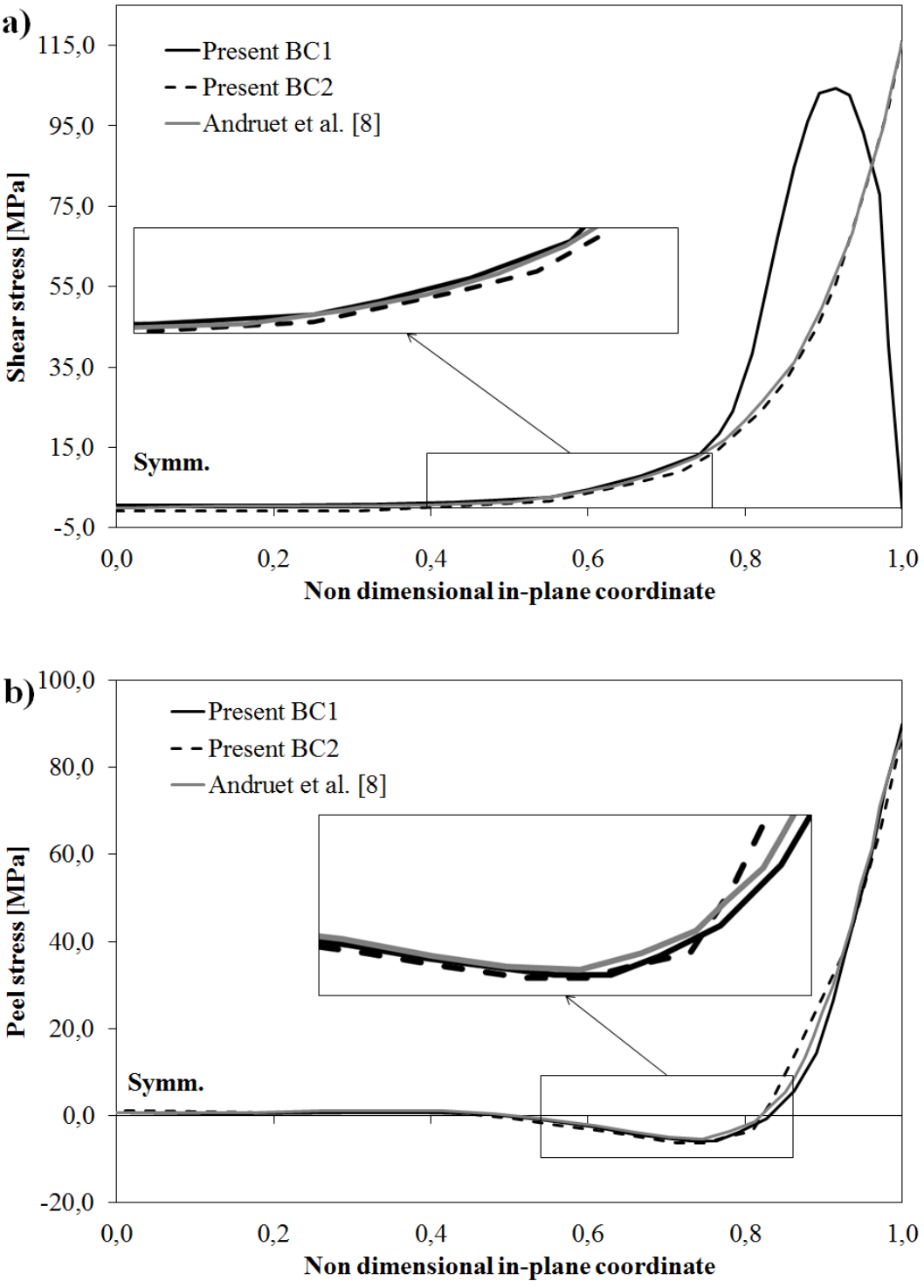

Fig. 3. Span-wise distribution of a) shear stress and b) peel stress by Andruet et al. [8] and by the present model considering different boundary conditions.

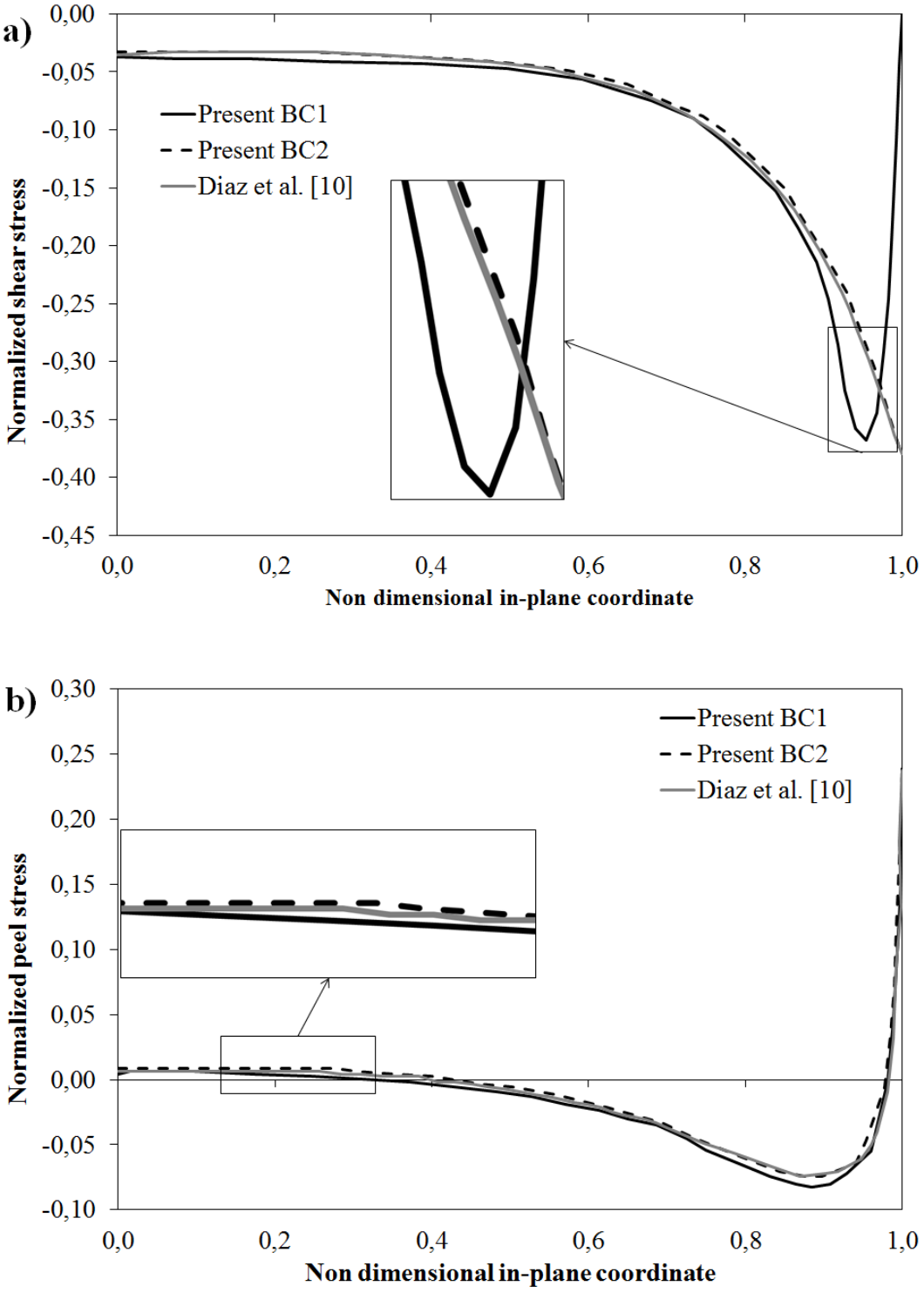

Fig. 4. Span-wise distribution of a) shear stress and b) peel stress by Diaz et al. [10] and by the present model using different boundary conditions and using SEUPT.

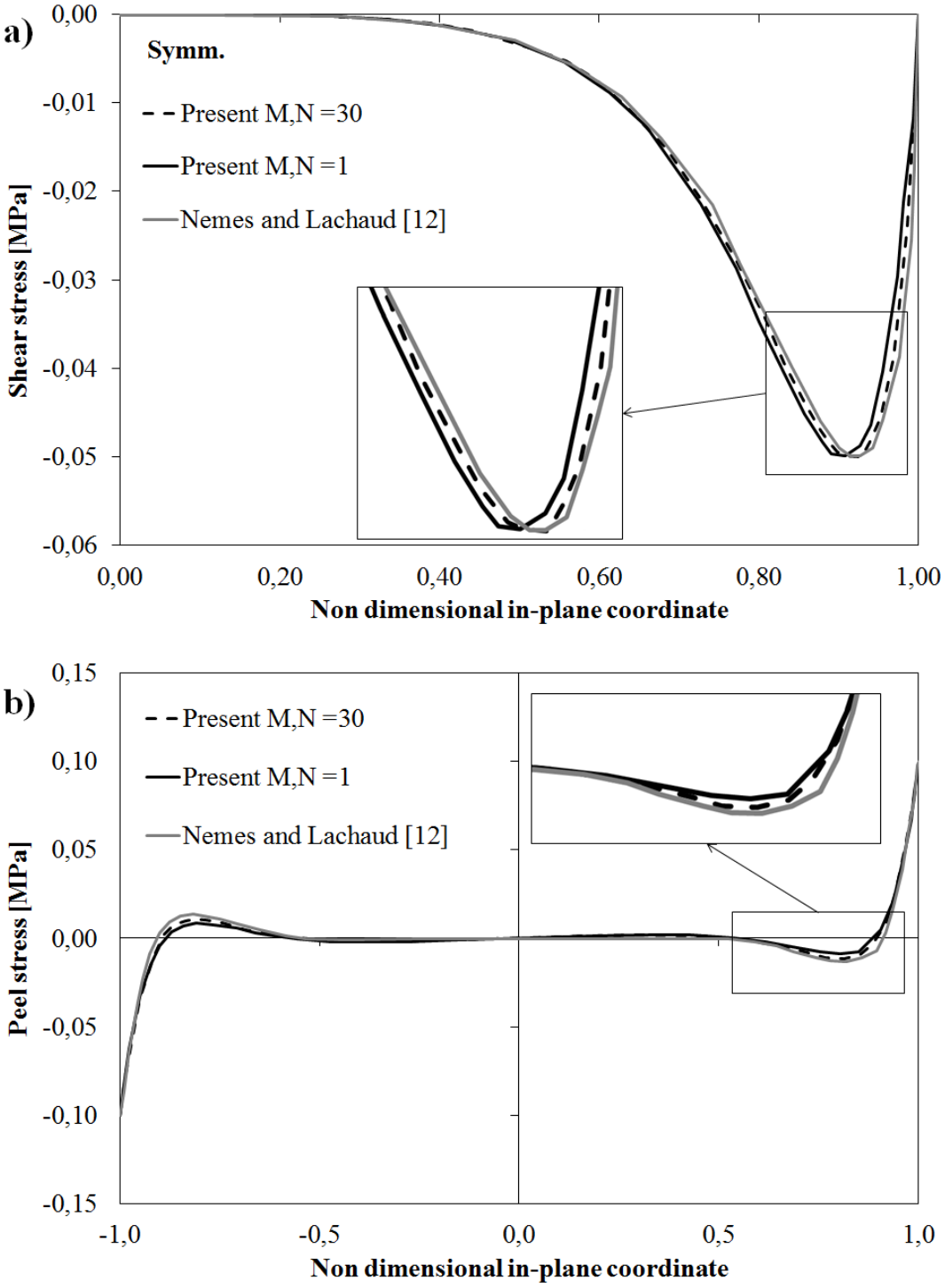

Fig. 5. Span-wise distribution of a) shear stress and b) peel stress by Nemes and Lachaud [12] and by the present model using different trial functions.

Prof Ugo Icardi graduated Summa cum Laude at Politecnico di Torino in 1982, and received his Ph.D. in 1986. He was first employed in the automotive sector, then as a staff member at the Department of Mechanical and Aerospace Engineering of Politecnico di Torino. His main research area is the simulation of the response of composite materials and smart structures, impact induced damage, progressive failure analysis and optimization techniques for spatially variable stiffness properties.

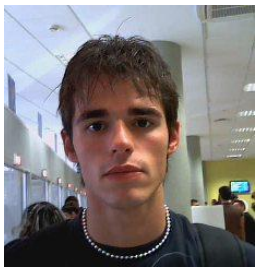

Dr Federico Sola graduated Summa cum Laude at Politecnico di Torino in October 2012 with a thesis entitled 'Efficient formulation of a model with adaptive kinematic for optimization of variable stiffness composites'. Currently he is Ph.D. student at Politecnico di Torino-Department of Mechanical and Aerospace Engineering. He has authored seven papers in co-operation with Prof Icardi dealing with modelling composites.